1

Grid-connected Renewable Energy Sources

In the face of energy challenge, the demand for new primary energy sources worldwide is evolving. But reserves of oil and fossil fuels in our planet are going to be exhausted in the near future. On the other hand, global warming becomes a more serious issue due to the greenhouse effect. The production of electrical energy from the oil, natural gas, coal, and nuclear sources is one of the main sources of greenhouse gases. For reducing the greenhouse gas emission and assuring the energy security, renewable energy sources (RESs) perform effective alternative solutions for clean and sustainable electrical power production.

In this chapter, the renewable power generation is briefly described. The principles for integration of wind power and solar power to the grid are presented. Then, the modeling procedure and control structures of the grid-connected wind and photovoltaic (PV) energy systems are emphasized. The problem of the primary energy intermittency is tackled and the PV and wind energy sources in hybrid configurations are also discussed. To investigate the proposed modeling and control schemes for the grid-connected wind and PV sources, some simulations and experimental results are provided, and finally the chapter is summarized.

1.1 Introduction

Today, global warming becomes more serious due to the greenhouse effect. Some emissions of greenhouse gases come from the human activities. The production and processing of electrical energy is one of the main sources of greenhouse gases. Directly or indirectly, environmental concerns dominate the thrust for an expanded deployment of renewable energy technologies. Climate change concerns, which arose during the late 1980s, have created a new input for clean, low-carbon energy technologies, such as renewable energy technologies. In December 1997, the Kyoto protocol was established

Microgrid Dynamics and Control, First Edition. Hassan Bevrani, Bruno Francois, and Toshifumi Ise.

in order to reduce global emissions of greenhouse gases. In the area of power generation, this protocol promotes RESs [1]. In the 11th session of the Paris to the 1997 Kyoto protocol, the 2015 United Nations Climate Change Conference in Paris drafted an agreement to set a goal of limiting global warming to less than 2 °C [2]. In the adopted version of the Paris agreement, the party will also pursue efforts to limit the temperature increase to 1.5 °C, which may require zero emissions sometime between 2030 and 2050.

Renewable energy is the energy generated from natural renewable resources such as sunlight, wind, ocean, hydropower, biomass, geothermal resources, biofuels, and hydrogen. The contribution potential of renewable energies in all countries is growing as the technologies mature. The RESs contribute to the diversity of energy supply portfolio and reduce the risks of continued/expanded use of fossil fuels and nuclear power. The RESs provide interesting options to consumers and are also the most environmentally benign energy supply options available in current and near-term markets. Moreover, the RESs contribute to a healthy economy, both in their contribution to the efficiency of the energy system and in the employment/investment opportunities that arise from continued rapid market growth.

Nowadays, governments and public organizations are concerned about the production of energy with technologies as clean as possible [3, 4]. As a consequence, the guidelines for future energy production are established according to the Kyoto protocol in 1997 and reemphasized by the Paris agreement in 2015. The energy production technologies based on hydro, wind, PV, and geothermal energies can be considered to be clean and renewable alternatives to the nonclean conventional technologies based on fossil fuels and nuclear fission. Among the clean technologies, PV and wind turbines have experienced a tremendous growth in the last years.

Wind power generators (WPGs) and solar power generators (SPGs) are able to provide the electrical power to supply a grid load. The energy conversion systems provided by wind turbines and PVs enable to extract the maximum wind/solar power by adjusting the wind turbine's rotational speed and solar plate effective surface. The obtained electrical power must be adapted before being sent to the grid. Therefore, an effective grid-following power balancing strategies must be used, while the WPGs/SPGs are working in the maximum power point tracking (MPPT) operating mode.

In order to reduce RES power variations, the energy storage systems (ESSs) can be used to build a hybrid power system (HPS). It is known that the HPS as a microgrid (MG) can be a good solution for the integration of distributed RESs in a power network. In this chapter, the WPG- and SPG-based hybrid systems modeling and control are presented. Some proper power control strategies such as "grid-following" and "power dispatching" strategies are also briefly addressed. In the performed power control strategies, the DC-bus voltage is regulated with the powers from the WPG/SPG and the ESSs.

1.2 Renewable Power Generation

The RESs convert natural energy sources (sunlight, wind, ocean, hydropower, biomass, geothermal resources, biofuels, and hydrogen) into consumable energy forms (electricity and heat), which are suitable to transport and to use. Solar, wind, water, biofuel, and geothermal power are known as the main sources of the renewable electric power.

Solar power: Solar power comes from the radiant light and heat from the sun. Sunlight can be converted directly into electricity by using PV panels or indirectly with concentrating solar power. The concentrating solar power normally focuses on the solar energy to boil water, which is then used in a steam turbine to provide electrical power. The PV technologies use semiconductor materials to convert sunlight into electricity. They have gradually dropped in price in the last two decades. The PV is now widely considered as a cost competitive option for many grid-connected, building-integrated, and off-grid applications as in telecommunications and local power supply.

Wind power: Wind power is considered as one of the most promising technologies for electricity production and the costs, with good wind regimes, that are comparable to fossil alternatives, particularly when the environmental benefit is considered. Airflow can run wind turbines for generating electricity. The rated power of present wind turbines ranges from 0.5 to 10 MW. The power output of a wind turbine depends on the wind speed and so, as the wind speed increases, the power output increases. The location of wind turbine installation is usually chosen in the areas with strong and constant winds, such as offshore and high-altitude sites. The offshore wind power experience shows that the mean wind speed is about 90% greater than the onshore one, so it may contribute more significantly to the supply of future power. Globally, the long-term technical potential of wind energy is believed to be several times the total current global energy production.

Water power: Water power can be exploited in a form of kinetic energy. Since water is about 800 times denser than the air, a slow flowing stream of water can yield considerable amount of energy. Water power exists in many forms. Hydroelectric energy is a term which is usually reserved for large-scale hydroelectric dams. Microhydro systems are hydroelectric power installations that typically produce up to 100 kW power, which are often used in water-rich areas as a remote area power supply. Ocean energy describes all the technologies to harness energy from the ocean and the sea including marine current power, ocean thermal energy conversion, and wave power.

Biofuel power: Plants use photosynthesis to grow and produce biomass. The biomass can be used directly as fuel or to produce biofuels. Agriculturally produced biomass fuels such as biodiesel, ethanol, and bagasse can be burned

in internal combustion engines or boilers. The biofuel is typically burned to release its stored chemical energy.

Geothermal power: Geothermal power comes from the heat of the earth itself, from hundreds of meters deep into the earth crust in some places of the globe or from tens of meters in geothermal heat pump in all the places of the planet. Geothermal technology is mostly used for thermal power production; the space heating is becoming increasingly important. Geothermal electricity production is a base load technology, which can be a low-cost option if the hot water or steam resource is at a high temperature and near the earth surface.

The *energy security*, *environment protection*, and *economic growth* are the main primary benefits of renewable energy options. Dependency of power energy on the limited stock of fossil fuels over an extended period is unsustainable and unsecure. Renewable energy may relieve the increasing need of the fossil fuels and reduces the mentioned dependency. On the other hand, the distributed capability of renewable energies brings the power production closer to the end-use, and minimizes energy transportation concerns and costs. Moreover, a greater use of RESs in the power energy portfolio may decrease overall generation costs relative to the probable risks [2]. Energy policies should focus on developing efficient generating portfolios that do not solely rely on stand-alone costs but also on expected portfolio risk, including year-to-year cost fluctuations.

Renewable energy has several important economic benefits. In developed countries, some economic benefits are employment creation and increased trade of technologies and services. An additional advantage is the insensitivity to fuel prices since they are free natural resources, which decreases the operational cost of renewable energy systems and reduces economic operation risks.

The initial investment in renewable-energy-based power generating systems can be considered as a drawback. It is often more expensive to build renewable energy systems than conventional energy systems, since the environmental deterioration has not yet been taken into account for the cost calculation. However, this investment cost will be reduced with the fast developing technologies (such as the development of computer industry and communication systems in the last three decades). Specific requirements of the site and the unpredictability of the generated power can be considered as other disadvantages of the RESs. The intermittent availability of the RESs means to pay a higher cost for regulation issues and maintaining reserve capacity. These quality and security problems have already been encountered in some countries with a high penetration of wind turbines.

1.2.1 Renewable Energy Development

Different kinds of renewable energy technologies have been established in the world markets. Some renewable energy technologies are becoming quickly competitive in growing markets, and some are widely recognized as the lowest cost options for the stand-alone and off-grid applications. The capital costs of certain renewable energy technologies have been obviously reduced over the last two decades and it is possible to be drastically reduced again over the next decade. During the last few years, the installed PV and wind powers dramatically increased.

The development of different renewable sources is limited by different constraints depending on their intrinsic characteristics. The hydropower and geothermal powers are naturally limited because of the lack of geographic sites. Biomass requires large storage places for the natural resources. That is why, a large development in PVs and wind turbines can be seen. But it is noteworthy that these RESs are intermittent power sources (Fig. 1.1a). The production of electricity from solar sources depends on the amount of light energy in a given location. Solar output varies throughout the days and seasons and is affected by cloud cover. Wind-generated power is also a variable resource, and the amount of produced electricity depends on wind speed, air density, and turbine characteristics. If the wind speed is too low (less than about 2.5 m/s), then wind turbines are not able to generate electricity. If it is too high (more than about 25 m/s), the turbines have to be shut down to avoid damage. Since the primary sources of renewable energy are uncertain, the RESs may produce a large amount of power when loads in the grid are very low, and they are not always available, such as solar power in the nighttime and wind power when the wind is not blowing.

The addition of intermittency increases the complexity of the use of RESs. The renewable-energy-based generations with intermittency decrease the reliability of a power system. The nature of intermittency is different for the respective renewable energy technologies, and this difference could be a relevant factor as far as mitigating the impacts of intermittency is concerned. As the percentage of intermittent generation capacity in a grid increases and becomes more significant, additional uncertainty to be created in the management of real-time demand and generation balance. This may require the increasing amount of conventional power reserve (spinning reserve) to manage the grid securely [5].

Most of RESs such as wind and PV generators may not individually participate to the grid management effectively, because they are dependent on the availability of the primary renewable sources. Most of the time, they may not work in their nominal capacity (Fig. 1.1a), and their maximum power variations

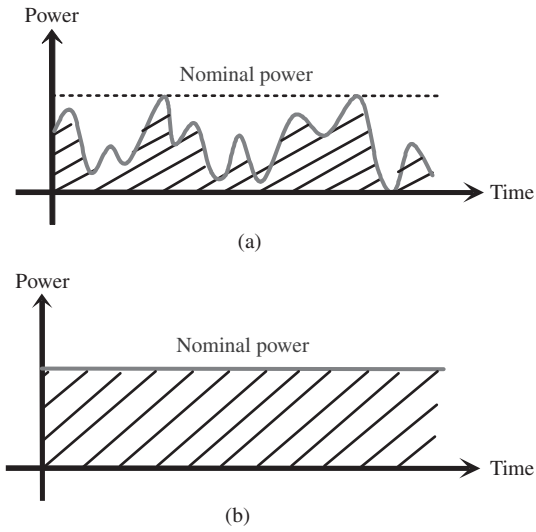

Figure 1.1 Power characteristics of renewable and conventional generators: (a) renewable power and (b) conventional power.

degrade the system reliability and efficiency. So without ESSs and more power generation systems, a high reliability and efficiency for a power system cannot be ensured.

In contrary, conventional power generators are easily controllable and can supply necessary power to satisfy the grid requirements. They can usually provide some ancillary services to the grid. They are mostly fossil and nuclear fueled and rely on the abundant fuel supply such as coal, oil, natural gas, or nuclear fuels. Most of the time, they can work at any power level below the nominal power (Fig. 1.1b) by controlling the fuel supply.

Energy storage devices can serve as backup power plants. They can be used to store or release electrical power such as an energy buffer, supporting the operation of sources, transmission, distribution, and loads. Therefore, as will be discussed later, they are useful to solve the problems of power intermittency and system low inertia in an RES-based power grid.

The combination of energy storage devices and RESs constitutes a hybrid power generator system, which can provide power not only for the local load but also can supply ancillary services to the main grid as the conventional generators [6]. Among all the RESs, the PV and wind turbines are known as the most popular renewable power sources.

1.3 Grid-connected Wind Power

In general, the WPGs can be classified into three categories [7].

1.3.1 Wind Power Generator Without Power Electronic Converters

Most of these topologies are based on a squirrel-cage induction machine (SCIM), which is directly connected to the grid. A soft starter is usually used to reduce the inrush current during start-up. Moreover, a capacitor bank is necessary for the reactive power compensation (Fig. 1.2a). By adding power electronic converters into the wind generator, a variable-speed wind generator can be achieved. Although the system complexity and the solution cost are increased, a better control of the converted primary power and of the grid connection can be obtained. For example, maximum power can be extracted from a large variation of wind speed. The use of power electronic converters in the wind generator can be further divided into two categories: systems using partial- and full-scale power electronic converters.

1.3.2 Wind Power Generator Using Partial-Scale Power Electronic Converters

A particular structure is based on a wounded rotor induction machine. An extra resistor controlled by power electronic converters is added in the rotor and gives a variable speed range of 2–4%. The power converter for the rotor resistor control is for low voltage but high currents. This solution also needs a soft starter and a reactive power compensator. Another solution is to use a back-to-back power electronic converter with the wounded rotor induction machine (WRIM), as shown in Fig. 1.2b.

In this case, a power converter connected to the rotor through slip rings controls the rotor currents. If the generator is running supersynchronously, the electrical power is delivered through both the rotor and stator. If the generator is running subsynchronously, the electrical power is only delivered into the rotor from the grid. A speed variation of 60% around synchronous speed may be obtained by the use of a power converter of 30% of the nominal power.

1.3.3 Wind Power Generator Using Full-Scale Power Electronic Converters

By implementing a full-scale power converter between the electrical machine and the utility grid, additional technical performances of the wind generator can be achieved. Normally, as shown in Fig. 1.2c, an SCIM or a synchronous machine (SM) is used in this configuration. By using a multipole wound rotor (or permanent magnet) synchronous machine, a high frequency of electrical quantities is generated and the gearbox can be eliminated (Fig. 1.2d).

In this section, a variable-speed WPG, as shown in Fig. 1.2c, is considered for extracting the maximum available wind power. Such kind of WPG supplies continuously varying powers, which depend on the intermittent and fluctuant wind velocity. When a large scale of WPGs is connected to the grid, stability problems occur due to the dependence of the power production on the wind condition [8–10].

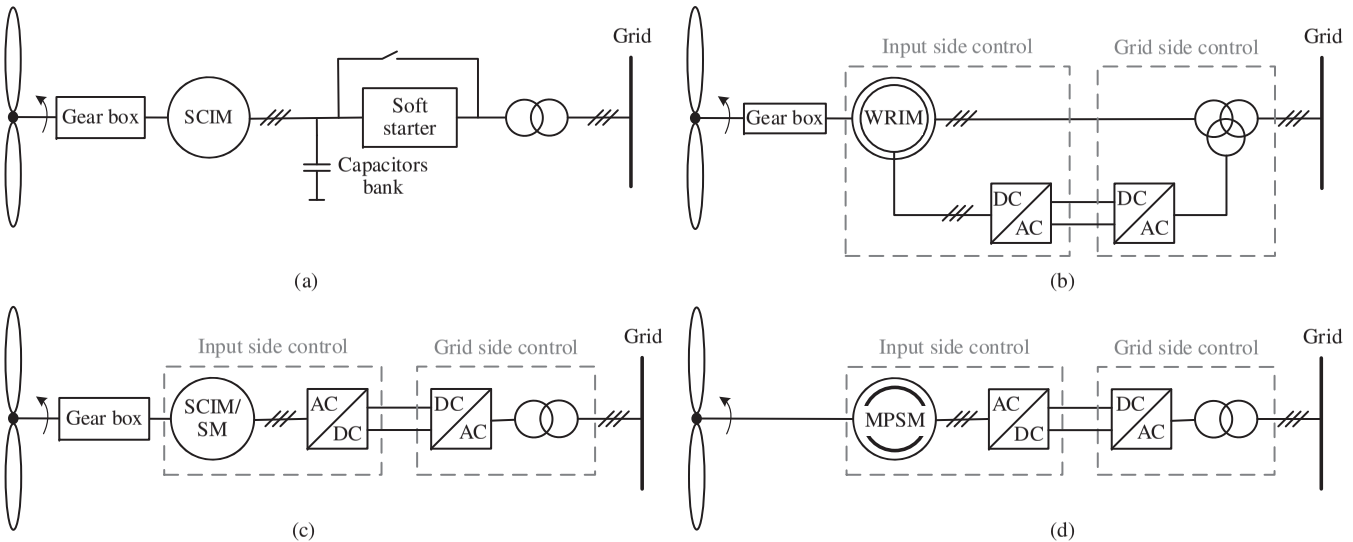

Figure 1.2 Wind generator with power electronics: (a) minimum electronics unit, (b) partial power converter, (c) full-scale power converter with gearbox, and (d) full-scale power converter without gearbox.

1.3.3.1 Wind Energy Conversion System: Modeling, Control, and Analysis

A classical wind energy conversion system consists of a three-blade turbine, a gearbox, an electrical machine, a three-phase rectifier, a DC-bus capacitor, a three-phase inverter, and line filters that are connected to the grid through a grid transformer (Fig. 1.3).

When the wind energy conversion system works in the MPPT strategy, a fluctuated power is delivered to the grid. A typical wind-speed-power profile recorded in a wind farm in the north of France is shown in Fig. 1.4 [11].

1.3.3.1.1 Electrical Conversion Chain Model Using equivalent average modeling of power electronic converters, the average model of the electrical power conversion chain can be obtained for the wind energy conversion system (Fig. 1.5). The grid with transformer is considered as three-phase voltage sources and the electrical machine is considered as three-phase current sources. Two back-to-back voltage source converters introduce control inputs for the power control. As the DC bus has a relatively slow dynamic, three different

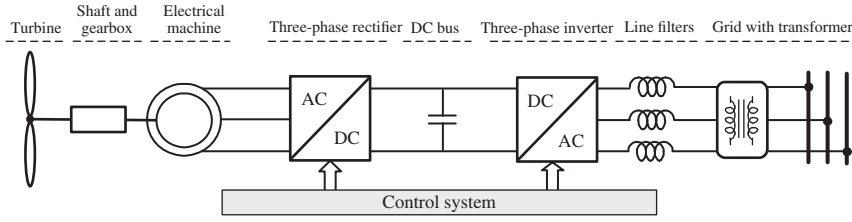

Figure 1.3 A conventional variable-speed WPG.

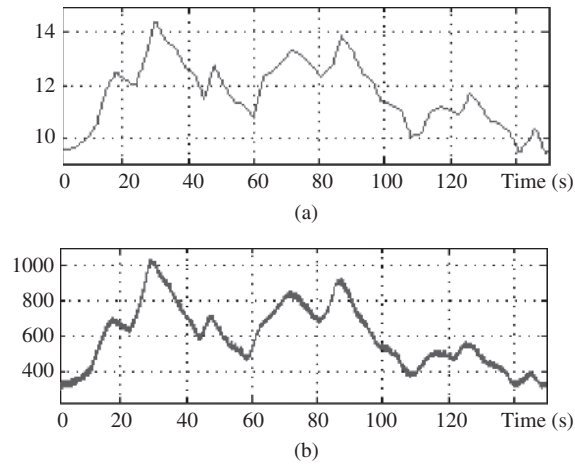

Figure 1.4 Real recorded wind speed-power pattern: (a) wind speed and (b) wind power.

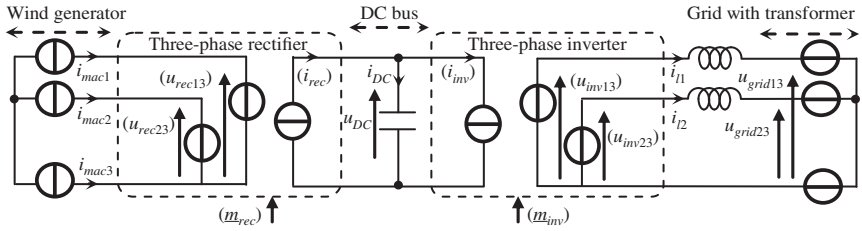

Figure 1.5 Equivalent average model of the power electronic converters.

subsystems with their inner dynamic and control tasks (wind generator, grid connection system, and the DC bus) can be considered.

Three-phase rectifier: The equivalent average model is used with average modulation functions. It yields the average values ($\langle \underline{u}_{rec} \rangle = [(u_{rec13}, u_{rec23}]^T$) of the modulated voltages from the DC-bus capacitor voltage (u_{DC}) and the average value ($\langle i_{rec} \rangle$) of the modulated current from the machine currents ($\underline{i}_{mac} = [i_{mac1}, i_{mac2}]^T$):

$$\begin{cases} \langle \underline{u}_{rec} \rangle = \langle \underline{m}_{rec} \rangle u_{DC} \\ \langle i_{rec} \rangle = \langle \underline{m}_{rec}^{\mathrm{T}} \rangle \underline{i}_{mac} \end{cases} \tag{1.1}$$

where $\underline{m}_{rec}$ is the vector of modulation functions of the grid inverter.

Three-phase inverter: The three-phase inverter is modeled in the same way. The average value of the modulated voltages ($\langle \underline{u}_{inv} \rangle = [(u_{inv13}, u_{inv23}]^T$) is calculated from the DC-bus voltage (u_{DC}) and the average value ($\langle i_{inv} \rangle$) of the modulated current from the line currents ($\underline{i}_l = [i_{l1}, i_{l2}]^T$):

$$\begin{cases} \langle \underline{u}_{inv} \rangle = \langle \underline{m}_{inv} \rangle u_{DC} \\ \langle i_{inv} \rangle = \langle \underline{m}_{inv}^{\mathrm{T}} \rangle \underline{i}_l \end{cases} \tag{1.2}$$

where $\underline{m}_{inv}$ is the vector of modulation functions of the grid inverter.

1.3.3.1.2 Wind Generator Model The modeling of the wind energy generation system is presented in detail in the block diagram shown in Fig. 1.6.

Wind: The wind is modeled by a mechanical source, which sets the wind velocity (v_{wind}) to the blades.

Turbine: The turbine is modeled as a mechanical converter. The torque (T_{tur}), which is produced by the turbine, depends on the wind velocity (v_{wind}) and the blade pitch angle (β):

$$T_{tur}(t) = \frac{1}{2} C_T(\lambda, \beta) \rho S_b R_b v_{wind}^2(t) \tag{1.3}$$

where S_b is the area that is swept by the blades, R_b is the blade length, ρ is the air density, C_T is the torque coefficient that is a nonlinear function of the

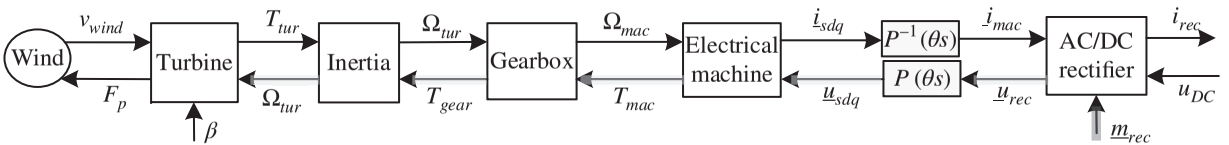

Figure 1.6 Block diagram of the considered wind energy generation system.

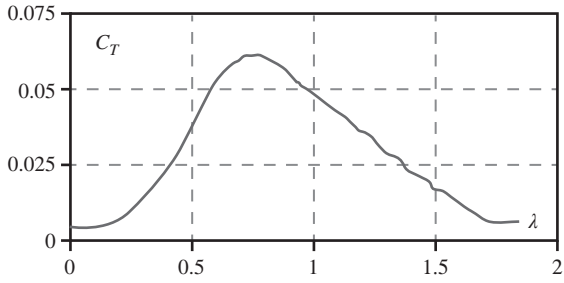

Figure 1.7 Blade characteristic: C_T versus λ for a fixed blade angle.

tip-slip ratio (λ) (Fig. 1.7), and λ is the tip-slip ratio depending on the wind velocity and the rotational speed (Ω_{tur}).

$$\lambda(t) = \frac{R_b \Omega_{tur}(t)}{v_{wind}(t)} \tag{1.4}$$

For the present study, a normal turbine operating with a constant pitch angle is considered.

Inertia: The shaft is an element with energy accumulation, which imposes the rotational speed (Ω_{tur}) with the torque difference between the blade torque (T_{tur}) and the gear torque (T_{gear}),

$$J_{shaft} \frac{d\Omega_{tur}(t)}{dt} = T_{tur}(t) - T_{gear}(t) - f_{shaft}\Omega_{tur}(t) \tag{1.5}$$

where the J_{shaft} is the equivalent inertia moment of the shaft and the f_{shaft} is the friction coefficient of the equivalent shaft.

Gearbox: The gearbox is a mechanical converter and adapts the low speed of the turbine with the high speed of the electrical machine. It yields the rotational speed (Ω_{mac}) and the torque (T_{gear}) through the gear ratio (m_{gear}):

$$\begin{cases} \Omega_{mac}(t) = m_{gear}\Omega_{tur}(t) \\ T_{gear}(t) = m_{gear}T_{mac}(t) \end{cases} \tag{1.6}$$

Electrical machine: The electrical machine can be generally modeled as an electromechanical converter with the rectifier voltages ($u_{rec} = [u_{rec13}, u_{rec23}]^T$) and the gear speed ($\Omega_{mac}$) as the inputs. The stator currents ($i_{mac} = [i_{mac1}, i_{mac2}]^T$) and the machine torque (T_{mac}) are the outputs.

For understanding the electrical machine dynamic, first one needs to use a mathematical transformation from phase-to-phase voltages ($\underline{u}_{rec}$) to machine line voltages. Then, the Park transformation expresses stator voltages and currents in a d–q rotational frame ($\underline{u}_{sdq}$):

$$\begin{cases} \underline{u}_{sdq} = P(\theta_s)\underline{u}_{rec} \\ \underline{i}_{mac} = P^{-1}(\theta_s)\underline{i}_{sdq} \end{cases} \tag{1.7}$$

where θ_s (or θ_{sdq}) is the angle of the rotating d–q frame with respect to the stator stationary frame. In the d–q frame, the equivalent stator windings set the stator currents ($\underline{i}_{sdq} = [i_{sd}, i_{sq}]^T$) as state variables, which are calculated with the stator voltages ($\underline{u}_{sdq} = [u_{sd}, u_{sq}]^T$) and the electromotive force (emf) ($\underline{e}_{sdq} = [e_{sd}, e_{sq}]^T$),

$$\begin{cases} L_s \frac{di_{sd}}{dt} = u_{sd} + e_{sd} - R_s i_{sd} \\ L_s \frac{di_{sq}}{dt} = u_{sq} - e_{sq} - R_s i_{sq} \end{cases} \tag{1.8}$$

R_s is the resistor of the stator winding and L_s is the cyclic inductor of the stator winding.

Finally, such as an electromechanical converter, it leads to the machine torque (T_{mac}) and the emf ($\underline{e}_{sdq}$) from the stator currents and the rotor's electrical angular speed (Ω_{mac}).

$$T_{mac} = \frac{3}{2}\rho(\phi_{rd} i_{sq} - i_{sd}\phi_{rq})$$

The rotor flux orientation is achieved by aligning the d-axis of the synchronous reference frame with the rotor flux vector ϕ_r. The resultant d- and q-axis rotor flux components are $\phi_{rq} = 0$ and $\phi_{rd} = \phi_r$.

$$T_{mac} = \frac{3}{2}\rho\phi_{rd} i_{sq} \tag{1.9}$$

$$\begin{cases} e_{sd} = L_s \Omega_{mac} i_{sq} \\ e_{sq} = L_s \Omega_{mac} i_{sd} \end{cases} \tag{1.10}$$

where ρ is the number of pole pairs and ϕ_{rd} is constant rotor flux of the permanent magnet.

1.3.3.1.3 Modeling of the Grid Connection

The modeling of the grid connection system is presented in Fig. 1.8.

Grid filter: The line currents ($\underline{i}_l$) are calculated from dynamic equations of the filter with the inverter phase-to-phase voltages ($\underline{u}_{inv}$) and the phase-to-phase grid voltages ($\underline{u}_{grid}$):

$$L_{line} \frac{d\underline{i}_l}{dt} = \frac{1}{3}\begin{bmatrix} 2 & -1 \\ -1 & 2 \end{bmatrix} (\underline{u}_{inv} - \underline{u}_{grid}) - r_{line}\underline{i}_l \tag{1.11}$$

where L_{line} is the equivalent inductor of the grid filter and r_{line} is the equivalent resistor in series of the grid filter. The electrical network with the grid transformer is considered as ideal sinusoidal phase-to-phase voltage sources $\underline{u}_{grid} = [u_{grid13}, u_{grid23}]^T$.

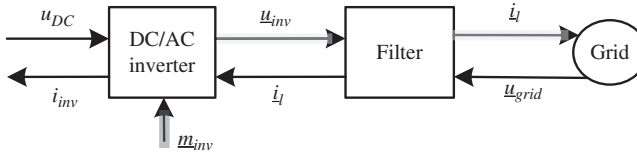

Figure 1.8 Block diagram of the grid connection system.

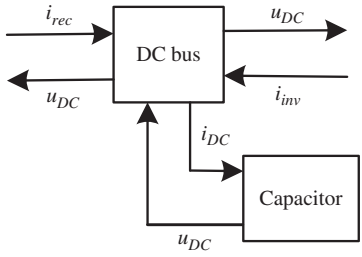

Figure 1.9 Block diagram of the DC bus.

1.3.3.1.4 Modeling of the DC Bus The model of the DC bus is presented in Fig. 1.9. In order to control the power exchanges around the DC bus, the DC coupling should be modeled in detail:

$$i_{DC} = i_{rec} - i_{inv} \tag{1.12}$$

where i_{rec} is the rectifier's modulated current and i_{inv} is the inverter's modulated current.

The DC-bus capacitor is an element with energy accumulation and its voltage is calculated from the dynamic equation:

$$C_{DC}\frac{du_{DC}}{dt} = i_{DC} \tag{1.13}$$

where C_{DC} is the DC-bus capacitor and u_{DC} is the DC-bus voltage.

1.3.3.1.5 Modeling of the Entire Wind Energy Conversion System The model of the entire wind energy conversion system can be obtained by combining all block diagrams (Figs 1.6, 1.8, and 1.9), as shown in Fig. 1.10.

1.3.3.2 Hierarchical Control Structure

The wind energy conversion system transfers power from the WPG to the electrical grid. Two power converters are used to regulate the power exchange. A hierarchical control structure, such as shown in Fig. 1.11, can be considered to implement the control system. Two switching control units (SCUs) and two automatic control units (ACUs) are used separately in the control system for the mentioned power converters. A common power control unit (PCU) and a common mode control unit (MCU) are used for the instantaneous power

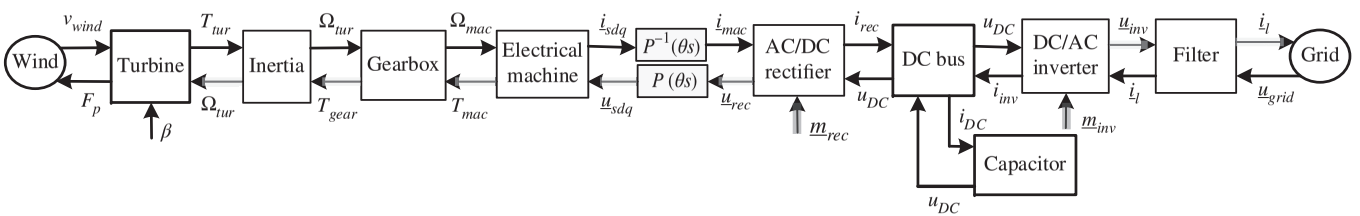

Figure 1.10 Block diagram of the entire wind energy conversion system.

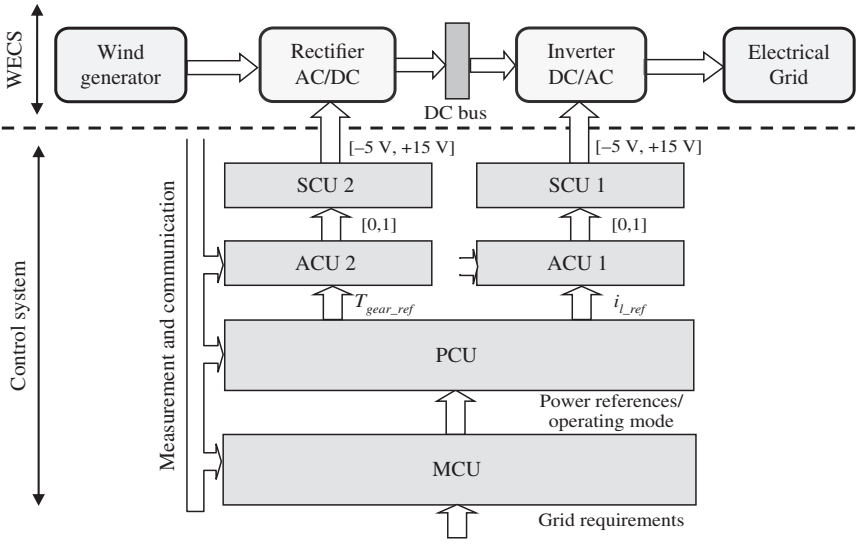

Figure 1.11 Hierarchical control structure of the wind energy conversion system.

balancing and the long-term energy management of the entire power system, respectively.

In the SCU of each converter, the insulated-gate bipolar transistors (IGBT) drivers and pulse width modulation (PWM) techniques are used to control the semiconductors in power electronic converters. The control algorithms in the ACU should be presented in order to highlight the physical quantities, which can be used for the power flow control among the different energy sources.

1.3.3.2.1 Wind Generator Control The electrical power versus speed curves of a typical wind turbine is given in Fig. 1.12. For example, if the wind velocity is v_1, the output power can be raised to the maximum value at point A by setting the mechanical speed to Ω_1. If the wind speed changes to v_2, the power output jumps to point B. For this wind velocity, the maximum power can be extracted by setting the speed at point C (Ω_2). This shows that, as the wind speed changes, the generator speed should track these changes in order to extract the maximum power. This is called MPPT strategy.

The block diagram of the wind energy conversion system modeling (Fig. 10) shows that the speed (Ω_{tur}) can be controlled by acting on two inputs: aerodynamic torque (T_{tur}) and torque of the generator (T_{gear}). As here we consider a normal operation with a constant pitch angle, the aerodynamic torque must be considered as a perturbation input (linked to the wind speed) for the system. So the turbine speed can be controlled by acting on the gearbox torque (T_{gear}) via the control input ($\underline{m}_{rec}$) of the power electronic converter.

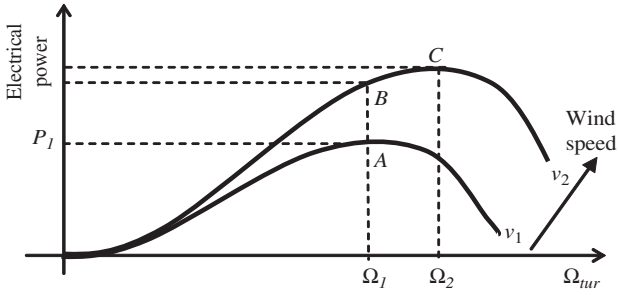

Figure 1.12 Turbine power-speed characteristic.

From the block diagram of the wind energy conversion system, an action chain appears from the control inputs ($\underline{m}_{rec}$) of the rectifier to the gear's mechanical torque (T_{gear}) (Fig. 1.10). The control scheme of the wind energy generation system is obtained by inverting this action chain (Fig. 1.13). It involves calculating the reference of the rectifier's duty ratios ($\underline{m}_{rec\_ref}$) according to a torque reference (T_{gear_ref}). It is composed of a torque control, a field-oriented control, and a rectifier control.

Torque control: The calculated mechanical torque reference (T_{gear_ref}) from an MPPT strategy is converted into the machine torque reference (T_{mac_ref}) by inverting (1.6):

$$T_{mac\_ref} = \frac{1}{m_{gear}} T_{gear\_ref} \tag{1.14}$$

Field-oriented control: A standard field-oriented control is used to control the electrical machine (Fig. 1.14) [12]. The inversion of (1.9) leads to the current references ($\underline{i}_{sdq\_ref} = [i_{sd\_ref}\ i_{sq\_ref}]^T$), i_{sq_ref} is obtained from the torque reference (T_{mac_ref}) with the constant rotor flux (ϕ_{rd}) of the permanent magnet and i_{sd_ref} is set to zero with a properly chosen frame orientation:

$$\begin{cases} i_{sq\_ref} = \frac{(2/3)}{p\phi_{rd}} T_{mac\_ref} \\ i_{sd\_ref} = 0 \end{cases} \tag{1.15}$$

As the stator windings are accumulation elements, closed-loop controllers are needed to invert (1.8):

$$\underline{u}_{sdq\_ref} = PI(\underline{i}_{sdq\_ref} - \underline{\hat{i}}_{sdq}) + \tilde{e}_{sdq} \tag{1.16}$$

where $PI(x_{ref}-x)$ is the controller of the variable x. In practice, the emf ($\underline{e}_{sdq}$) cannot be measured, but it can be estimated through the sensed rotor's rotational speed (Ω_{mac}) by using (1.10):

$$\begin{cases} \tilde{e}_{sd} = L_s \Omega_{mac} \hat{i}_{sq} \\ \tilde{e}_{sq} = L_s \Omega_{mac} \hat{i}_{sd} \end{cases} \tag{1.17}$$

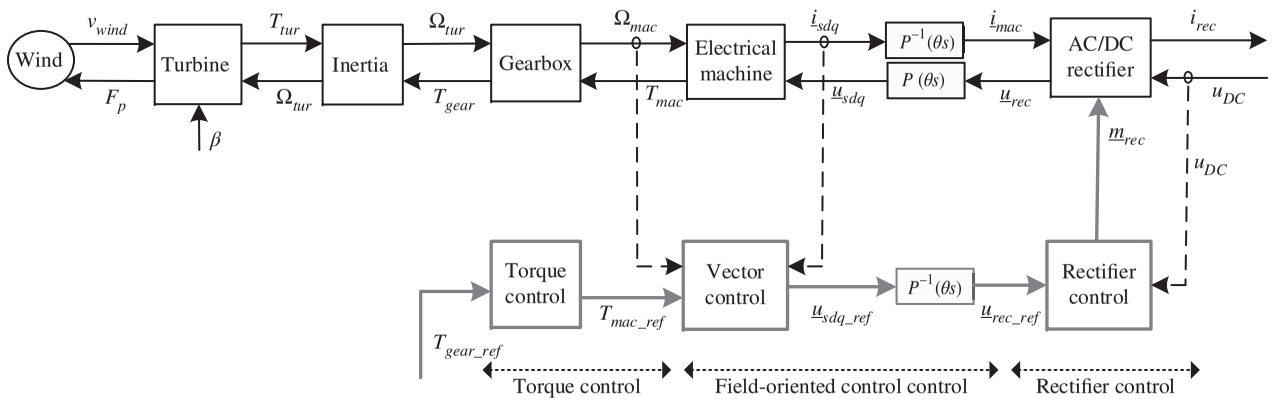

Figure 1.13 Control scheme of the wind energy generation system.

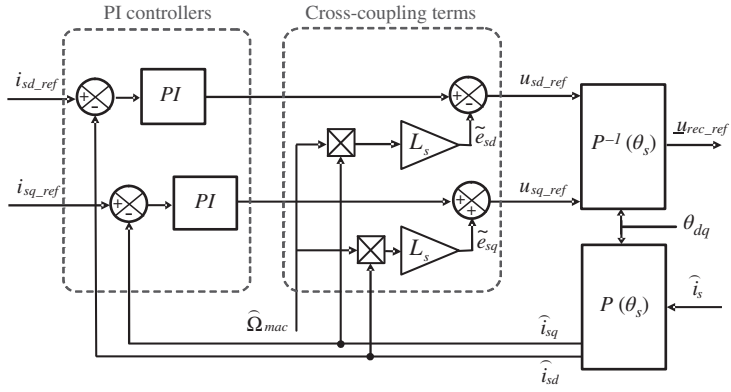

Figure 1.14 Block diagram of the oriented field control of the electrical machine.

Finally by inverting (1.7), the inverse Park transformation ($P^{-1}(\theta_s)$) leads to the references of the rectifier voltages ($\underline{u}_{rec\_ref}$):

$$\underline{u}_{rec\_ref} = P^{-1}(\theta_s)\underline{u}_{sdq\_ref} \tag{1.18}$$

Rectifier control: The reference modulation functions $\underline{m}_{rec\_ref}$ are obtained by inversion of (1.1) through the measurement of the DC-bus voltage u_{DC}:

$$\underline{m}_{rec\_ref} = \frac{1}{\hat{u}_{DC}}\underline{u}_{rec\_ref} \tag{1.19}$$

1.3.3.2.2 Grid Connection Control Considering the block diagram of the grid connection system (Fig. 1.8), a path from the control inputs ($\underline{m}_{inv}$) of the inverter to the line currents ($\underline{i}_l$) can be seen. The control scheme of the grid connection system is obtained by inverting this path (Fig. 1.15). It involves calculating the reference of the inverter's duty ratios ($\underline{m}_{inv\_ref}$) according to the line currents' references ($\underline{i}_{l\_ref}$).

Line current control: The grid is a voltage source ($\underline{u}_{grid}$), so the line current should be controlled in order to regulate the exchanged power with the grid. In order to control this current, a current controller is needed with a Park transformation (P) and an inverse Park transformation (P^{-1}) as shown in Fig. 1.16:

$$\begin{aligned} &\underline{u}_{inv\_ref} = P^{-1}(\theta_{dq})\,\underline{u}_{inv\_dq\_ref} \\ &\begin{cases} u_{inv\_d\_ref} = PI(i_{l\_d\_ref} - i_{l\_d}) + \hat{u}_{grid\_d} - \tilde{e}_{lq} \\ u_{inv\_q\_ref} = PI(i_{l\_q\_ref} - \underline{i}_{l\_q}) + \hat{u}_{grid\_q} + \tilde{e}_{ld} \end{cases} \end{aligned} \tag{1.20}$$

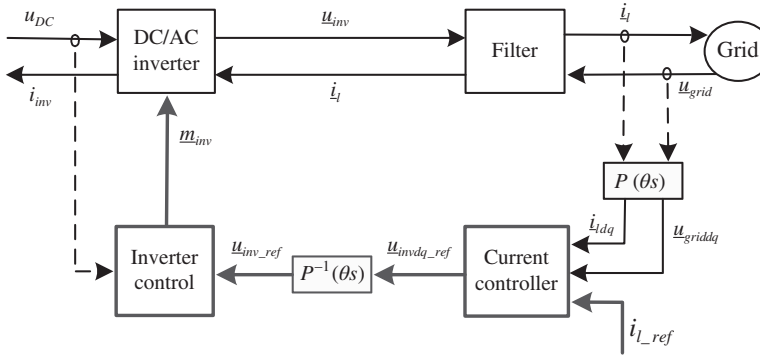

Figure 1.15 Control scheme of the grid connection system.

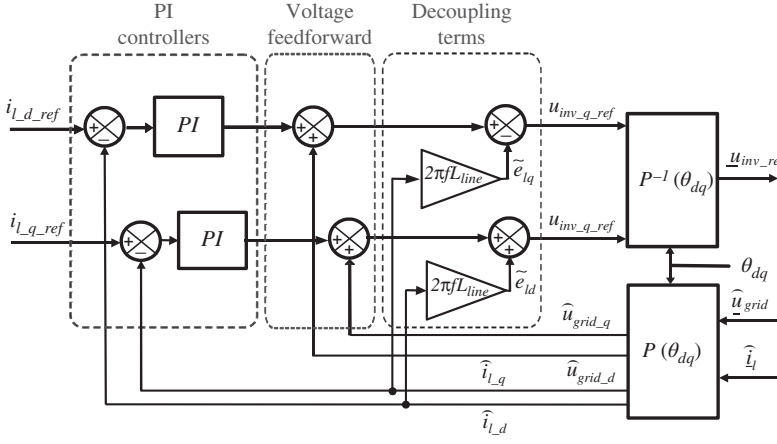

Figure 1.16 Block diagram of the line current control in the grid connection system.

where $\underline{i}_{l\_dq\_ref} = P(\theta_{dq})\underline{i}_{l\_ref}$, $\underline{\hat{i}}_{l\_dq} = P(\theta_{dq})\underline{\hat{i}}_l$, $\underline{\hat{u}}_{grid\_dq} = P(\theta_{dq})\underline{\hat{u}}_{grid}$, $\tilde{e}_{lq} = 2\pi f L_{line}\hat{i}_{l\_q}$, $\tilde{e}_{ld} = 2\pi f L_{line}\hat{i}_{l\_d}$, and f is the frequency of the grid voltage.

Inverter control: The modulation functions of the inverter are obtained by inverting (1.2):

$$\underline{m}_{inv\_ref} = \frac{1}{\hat{u}_{DC}}\underline{u}_{inv\_ref} \tag{1.21}$$

1.3.3.2.3 DC Bus Control The wind energy conversion system can be decomposed into three independent subsystems if the DC-bus voltage is constant. The DC-bus voltage should be well regulated for the stability of the grid connection

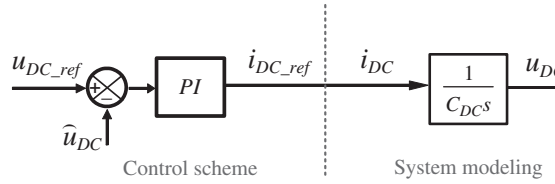

Figure 1.17 Control scheme of the DC bus.

because it is used in a division operator in the converter control algorithms ((1.19) and (1.21)), so a voltage controller is needed (Fig. 1.17):

$$i_{DC\_ref} = PI(u_{DC\_ref} - \widehat{u}_{DC}) \tag{1.22}$$

1.3.3.2.4 Control of the Entire Wind Energy Conversion System The control scheme of the entire wind energy conversion system is obtained by combining all the control schemes presented earlier. The result is drawn in Fig. 1.18. The corresponding block diagram of the ACUs is shown in Fig. 1.19.

1.3.3.2.5 Power Control Unit In the studied wind energy conversion system, all power exchanges are performed via the DC-bus (Fig. 1.20) and have an impact on the DC-bus voltage:

$$\frac{dE_{DC}}{dt} = C_{DC}u_{DC}\frac{du_{DC}}{dt} = u_{DC}i_{DC} = p_{DC} = p_{wg} - p_{gc} \tag{1.23}$$

where E_{DC} is the stored energy in the DC-bus capacitor, p_{DC} is the exchanged power with the DC-bus capacitor, p_{wg} is the injected power into the DC bus from the wind generator, and p_{gc} is the extracted power from the DC bus into the grid.

- **General layout**
  The PCU can be divided into two levels: the power control level (PCL) and the power sharing level (PSL). The PCL involves calculating the reference of the related quantities (T_{gear_ref}, $\underline{i}_{DC\_ref}$, $\underline{i}_{l\_ref}$) from the power references (p_{wg_ref}, p_{DC_ref}, p_{g_ref}, q_{g_ref}). The PSL coordinates the power flow exchanges among the different energy sources.
- **Power control level**
  Each controlled quantities implies a power, which is calculated in Table 1.1. For the wind generator, an MPPT strategy is used to extract the maximum power. The power reference (p_{wg_ref}) can be set by calculating the corresponding torque reference (T_{gear_ref}) with the sensed value of the rotational speed (Ω_{tur}) according to the inverse equation (iii_c). The powers, which are exchanged with the grid, can be calculated through the "two-wattmeter" method with the equation (ii) and the line current references are calculated by the inverse equations (ii_c). The output of the DC-bus voltage control loop is a reference for the required DC current (i_{DC_ref}), and its product with

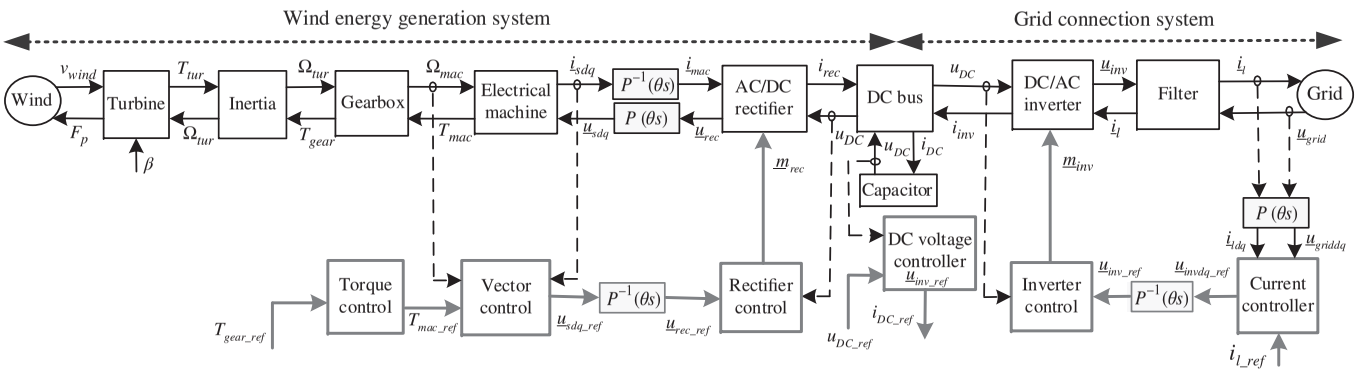

Figure 1.18 Control scheme of the entire wind energy conversion system.

the measured DC-bus voltage (u_{DC}) gives the necessary power reference (p_{DC_ref}) for the DC-bus voltage regulation according to (i_c).

- **Power sharing level**
  The choke filters are sized to obtain a small voltage drop across them and their losses and reactive powers are small. Moreover, these powers will be considered as disturbances and can be attenuated by the various closed-loop controls used. So we will not discuss in detail the power estimation of losses and compensation algorithms in order to focus on the power balancing algorithms.

We can assume that the wind power (p_{wg}) is divided into two parts (Fig. 1.21). One part (p_{DC}) is sent to the DC-bus capacitor. The other part is sent to the grid (p_g). The power exchange can be expressed as

$$p_g = p_{wg} - p_{DC} \tag{1.24}$$

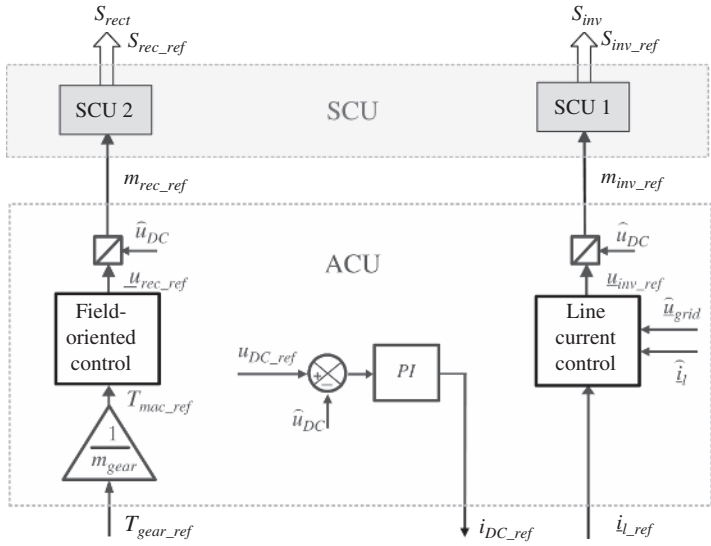

Figure 1.19 Block diagram of the automatic control units for the wind energy conversion system.

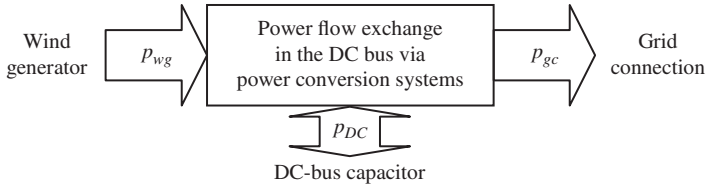

Figure 1.20 Power flow exchanges around the DC bus.

Table 1.1 Power calculation and control algorithms for the wind energy conversion system.

Energy source	Power calculation	Power control
DC-bus capacitor	$p_{DC} = u_{DC} i_{DC}$ (i)	$p_{DC\_ref} = \widehat{u}_{DC} i_{DC\_ref}$ (i_c)
Grid connection	$\begin{cases} p_g = u_{13} i_1 + u_{23} i_2 \\ q_g = \sqrt{3}(u_{13} i_1 - u_{23} i_2) \end{cases}$ (ii)	$\begin{cases} i_{l1\_ref} = \dfrac{(2\widehat{u}_{13} - \widehat{u}_{23}) p_{g\_ref} + \sqrt{3}\widehat{u}_{23} q_{g\_ref}}{2\widehat{u}_{13}^2 - 2\widehat{u}_{13}\widehat{u}_{23} + 2\widehat{u}_{23}^2} \\ i_{l2\_ref} = \dfrac{(2\widehat{u}_{23} - \widehat{u}_{13}) p_{g\_ref} - \sqrt{3}\widehat{u}_{13} q_{g\_ref}}{2\widehat{u}_{13}^2 - 2\widehat{u}_{13}\widehat{u}_{23} + 2\widehat{u}_{23}^2} \end{cases}$ (ii_c)
Wind generator	$p_{wg} = \Omega_{tur} T_{gear}$ (iii)	$T_{gear\_ref} = \dfrac{1}{\widehat{\Omega}_{tur}} p_{wg\_ref}$ (iii_c)

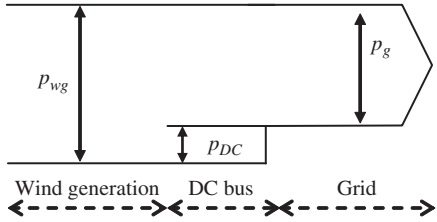

Figure 1.21 Power flow exchange inside the wind energy conversion system.

The wind generator is connected to a three-phase rectifier and various control strategies can be used. For example, when the wind velocity is not too high, the wind generator can work with an MPPT strategy to improve the global energy efficiency. When the wind velocity becomes too high, the wind generator can work with the rated power strategy by reducing the power efficiency for security reasons. In our study, we assume that the wind velocity is medium and we use an MPPT strategy in the form of a searching algorithm for the maximum power as shown in Fig. 1.12. Therefore, with the fluctuant wind, the wind power is very fluctuant. This fluctuant power is rectified and sent to the DC bus. Hence, a "grid-following" power balancing strategy should be used (Fig. 1.22) because the availability of the wind power is not ensured for the DC bus control, and the DC-bus voltage is regulated by the line current controller through the three-phase inverter. The wind power (p_{wg}) must be seen as a fluctuant disturbance. In order to regulate the DC-bus voltage, the only way is to use the grid power (p_g), as shown in the closed loop ($u_{DC\_ref} \rightarrow p_{DC\_ref} \rightarrow p_{g\_ref} \rightarrow m_{inv} \rightarrow p_g \rightarrow p_{DC} \rightarrow u_{DC}$) in Fig. 1.22.

So the grid power reference (p_{g_ref}) is obtained by taking into account the DC-bus power reference (p_{DC_ref}) for the voltage regulation and the estimated wind power $\tilde{p}_{wg}$. In practice, we can set $\tilde{p}_{wg} = p_{wg\_ref}$. The hierarchical control

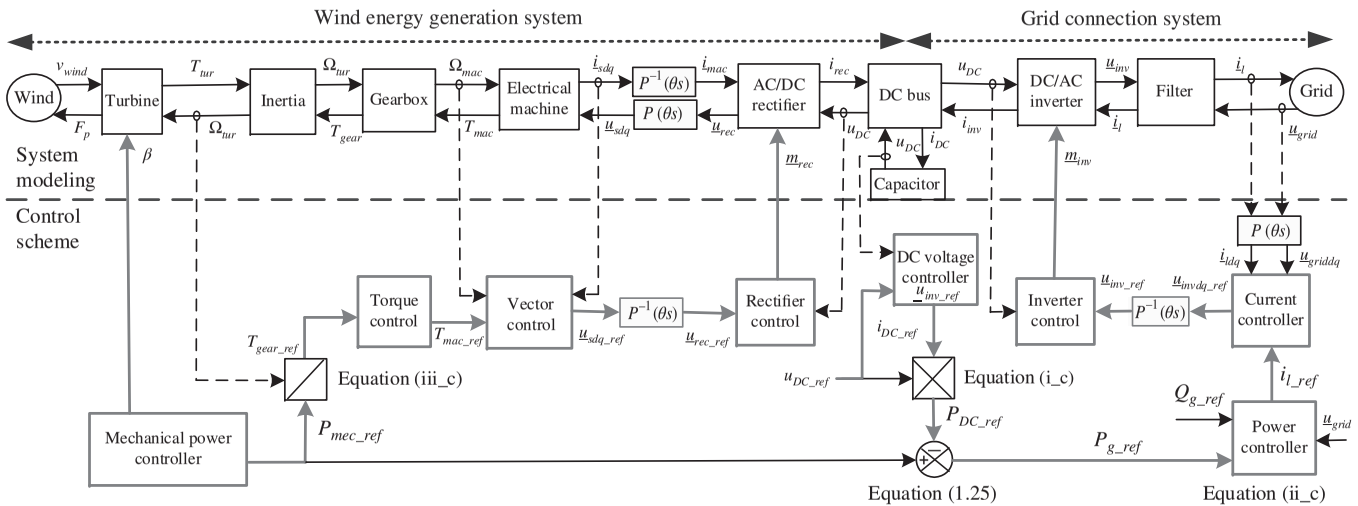

Figure 1.22 Multilevel representation of the wind energy conversion system.

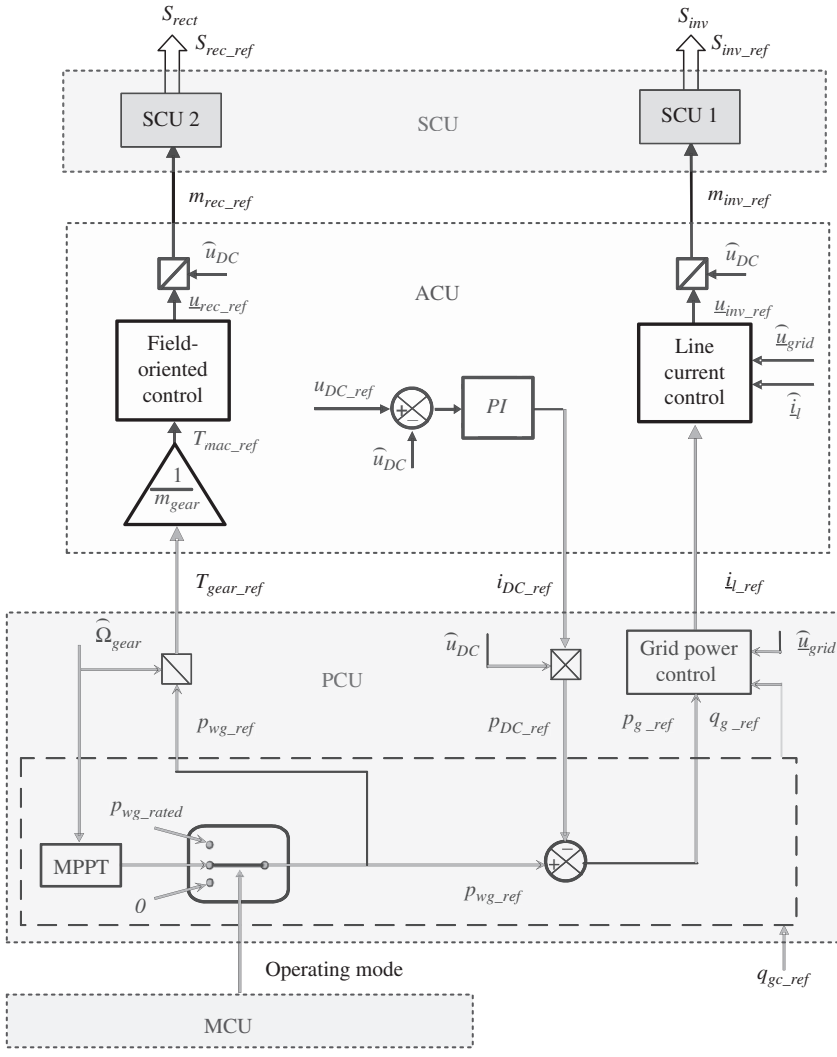

Figure 1.23 Block diagram of the hierarchical control for the wind energy conversion system.

system of the wind energy conversion system is then extended as shown in the block diagram of Fig. 1.23.

$$p_{g\_ref} = \tilde{p}_{wg} - p_{DC\_ref} \tag{1.25}$$

1.3.3.2.6 Mode Control Unit The operating mode of the wind generator depends on the wind speed condition and the grid requirements (Fig. 1.23).

The wind generator can work normally while the grid capacity is large enough to receive the fluctuant wind power without much impact. If the wind speed is low or medium, the wind generator works in an MPPT strategy. Otherwise, the wind generator should be limited with the rated power value (p_{wg_rated}) with high wind speed, or even be shut down with extremely high wind speed for security reasons.

$$p_{wg\_ref} = \begin{cases} \text{MPPT}(\Omega_{tur}) & \text{with weak or medium wind} \\ p_{wg\_rated} & \text{with strong wind} \\ 0 & \text{with extremely strong wind} \end{cases} \tag{1.26}$$

These strategies can be switched in the PCU by a signal (*operating mode*) coming from the MCU (Fig. 1.23).

1.3.3.3 Simulation and Experimental Examination

1.3.3.3.1 Hardware and Software Implementation To show the validity of the proposed model, wind generator emulators have been used in the laboratory. In this section, a simplified version is presented to obtain the same power variation as from the real wind generator (Fig. 1.4). In order to have a flexible and "easy-to-use" wind energy conversion system for testing control algorithms, an emulator with a reduced rated power (1.2 kW) has been developed.

The wind power emulator is a controllable power source, which must provide the same power profile as the wind energy generation system. So, the wind generator in Fig. 1.5 is replaced experimentally by the wind power emulator as shown in the equivalent average modeling (Fig. 1.24).

In this case, the average value of the modulated current from the chopper ($\langle i_{m\_wg} \rangle$) in Fig. 1.24 is proportional to the average value of the modulated current from the three-phase rectifier ($\langle i_{rec} \rangle$) in Fig. 1.5. The power electronic stage of the wind power emulator is implemented with a step-up power conversion circuit (Fig. 1.25), including a constant DC voltage source (120 V), a choke filter (20 mH), and a DC chopper. By controlling the current (i_{wg}) of the filter

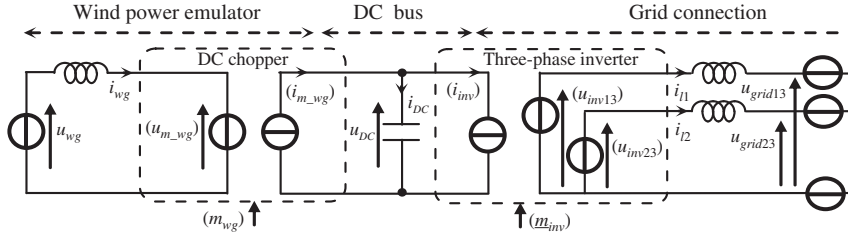

Figure 1.24 Equivalent average modeling of the power conversion chain with a wind power emulator.

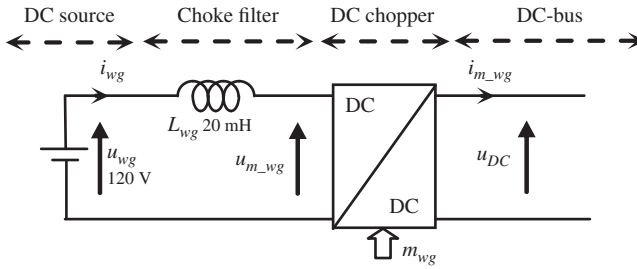

Figure 1.25 Power electronic stage of the wind power emulator.

inductor, the power of the emulator can be well controlled through the duty ratio (m_{wg}) as control input.

The dynamic representation and relevant equations can be easily obtained as described in the previous sections. For modeling the DC chopper, the choke filter is an element with accumulation and the state variable is the current (i_{wg}):

$$L_{wg}\frac{di_{wg}}{dt} = \widehat{u}_{wg} - u_{m\_wg} \tag{1.27}$$

where L_{wg} is the inductor and u_{m_wg} is the modulated voltage of the chopper. The chopper is a conversion element:

$$\begin{cases} u_{m\_wg} = m_{wg}\widehat{u}_{DC} \\ i_{m\_wg} = m_{wg}\widehat{i}_{wg} \end{cases} \tag{1.28}$$

where m_{wg} is the duty ratio of the chopper and u_{DC} is the DC-bus voltage.

The power electronic stage of the emulator performs a path between the control input (m_{wg}) and the choke current (i_{wg}). The objective is to control this current. The control scheme of the wind power emulator is obtained by inverting this path. So a converter controller and a current controller are required.

A current controller is needed to make equal the inductor current (i_{wg}) to a reference value (i_{wg_ref}):

$$u_{m\_wg\_ref} = \widehat{u}_{wg} - PI(i_{wg\_ref} - \widehat{i}_{wg}) \tag{1.29}$$

A converter controller is obtained by inverting (1.28):

$$m_{wg\_ref} = \frac{1}{\widehat{u}_{DC}}u_{m\_wg\_ref} \tag{1.30}$$

The generated power can be described as follows:

$$p_{wg} = u_{wg}i_{wg} \tag{1.31}$$

Then, this power reference (p_{wg_ref}) for the emulator leads to a current reference (i_{wg_ref}) for the control system.

$$i_{wg\_ref} = \frac{1}{\widehat{u}_{wg}} p_{wg\_ref} \tag{1.32}$$

In normal operation, the DC-bus voltage is regulated to a prescribed constant value and then from (1.24), we obtain

$$p_g = p_{wg} \tag{1.33}$$

So the objective is to make the produced power from the emulator equal to a previously recorded wind power profile (Fig. 1.4),

$$p_{wg\_ref} = p_{g\_record} \tag{1.34}$$

The "wind power profile," which is implemented in the digital signal processor (DSP), sets this power reference (p_{wg_ref}) according to the recorded wind speed profile (Fig. 1.4). The experimental test bench is built with a 1.2 kW rated power; thus, the coefficient (k_{wg}) is adapted to have a wind power profile ($p_{wg\_ref} = k_{wg} p_{wg\_ref}$) below 1.2 kW. The grid connection system is experimentally implemented with a wind power emulator through a DC-bus capacitor (2300 μF), a three-phase inverter, three line filters (10 mH), and a three-phase grid transformer. The implementation of the wind energy conversion experimental test bench is shown in Fig. 1.26.

The modeling and control is obtained by replacing the wind energy generation system by the wind power emulator using the proposed modeling and control scheme (Fig. 1.22). The representation model of the entire experimental test bench can be drawn as shown in Fig. 1.27. The proposed hierarchical control system (Fig. 1.23) is experimentally applied and tested with the real DC bus and grid connection system by taking into account the fluctuant wind power.

1.3.3.3.2 Simulation and Experimental Results In order to validate our mathematical modeling and control design, it is first simulated for the given case study in the MATLAB/Simulink™ software environment. It can be seen that the obtained simulated active power (p_g) in Fig. 1.28a is very close to the recorded grid active power (Fig. 1.4). Hence, this mathematical model gives us the same power dynamics as from a real wind generator. Moreover, we have now some knowledge about the internal physical quantities and also about the different control functions.

The grid connection test of the wind energy conversion system is performed with the same wind power profile during 150 s. The experimental results are compared with the previous simulation results. We can see that the similar power profile (Fig. 1.28b) can be generated as the recorded wind power profile (Fig. 1.4). The DC-bus voltage is well regulated (around 400 V) by the line current control loop in a "grid-following" power balancing strategy. The emulated

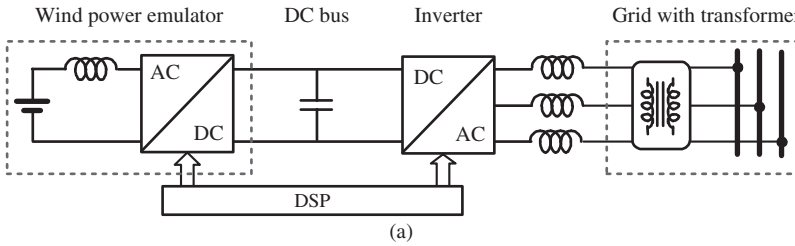

(a)

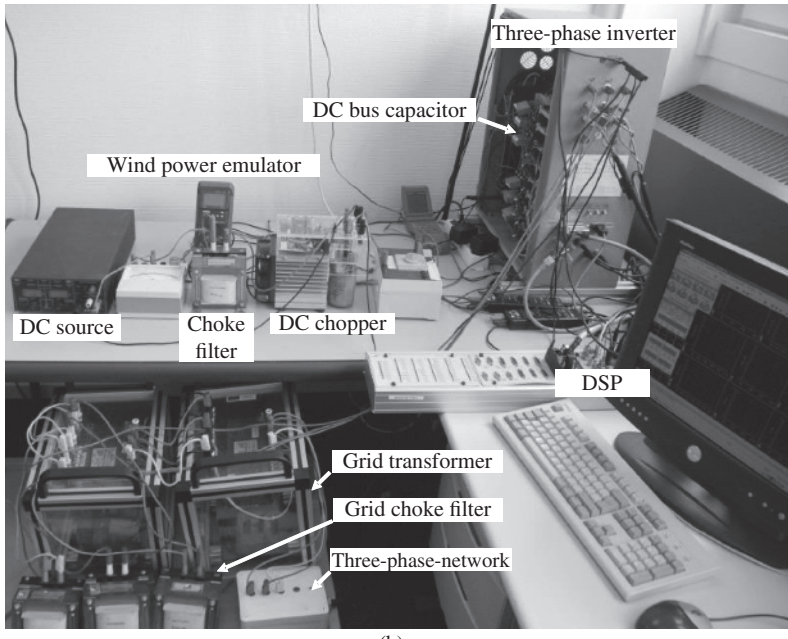

(b)

Figure 1.26 Implementation of the wind energy conversion experimental test bench; (a) block diagram and (b) laboratory experiment.

fluctuant wind power is totally delivered to the grid through the three-phase inverter.

This experimental test bench enables us to have similar power dynamics and characteristics as a real wind generator. We will use it to validate our proposed improvement in order to design a wind-based active generator. The fluctuant power from the wind generator depends entirely on the wind condition, but not on the grid's requirements. Therefore, the wind energy conversion system working in MPPT strategy behaves like a passive generator. It cannot supply smooth powers to the grid and cannot supply any ancillary services for the power system. It can only generate continuously varying powers depending on

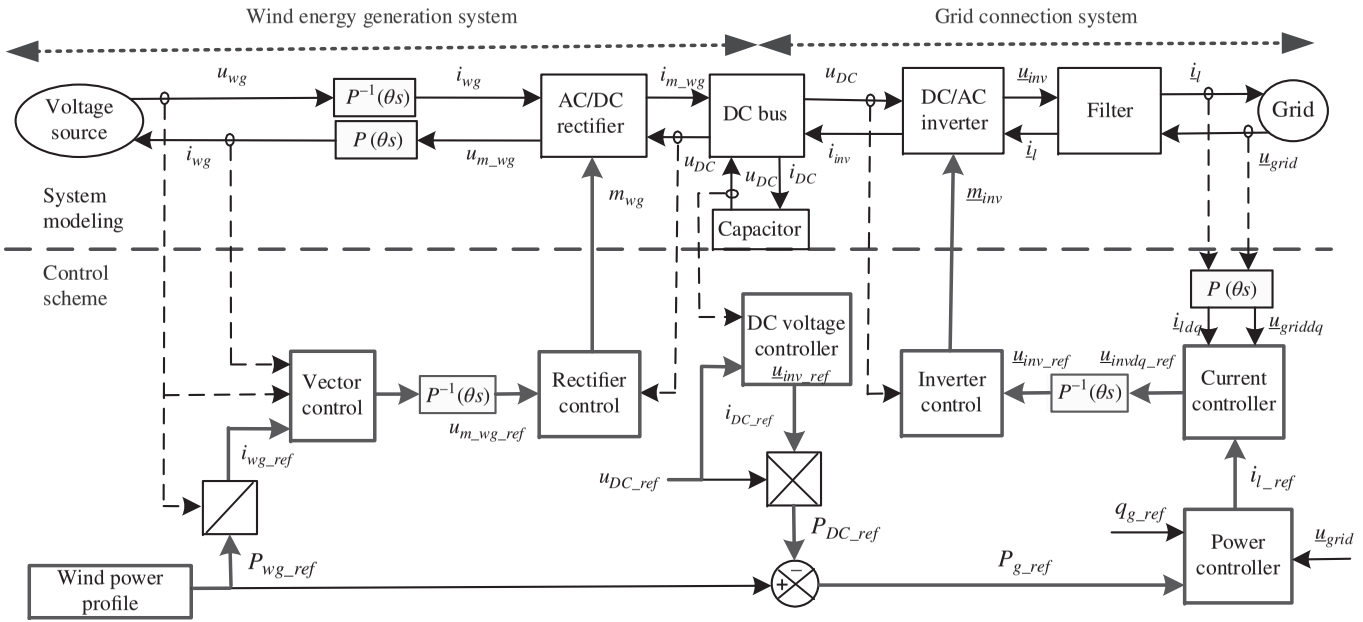

Figure 1.27 Model representation of the wind energy conversion experimental test bench.

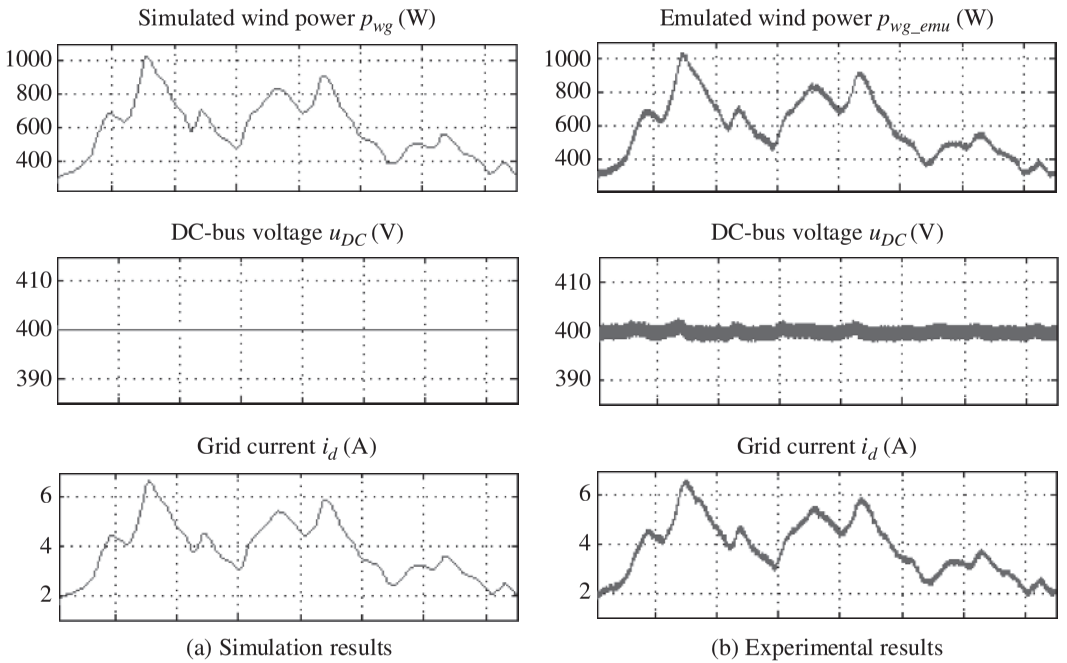

Figure 1.28 Test results of the wind energy conversion experimental test bench.

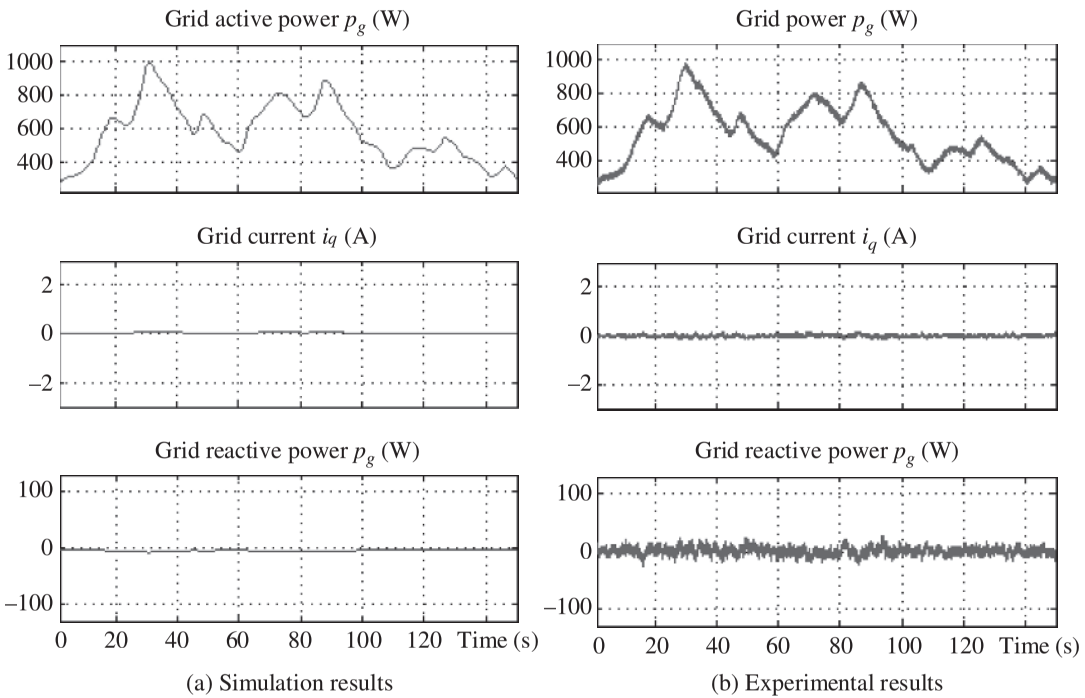

Figure 1.28 (*Continued*)

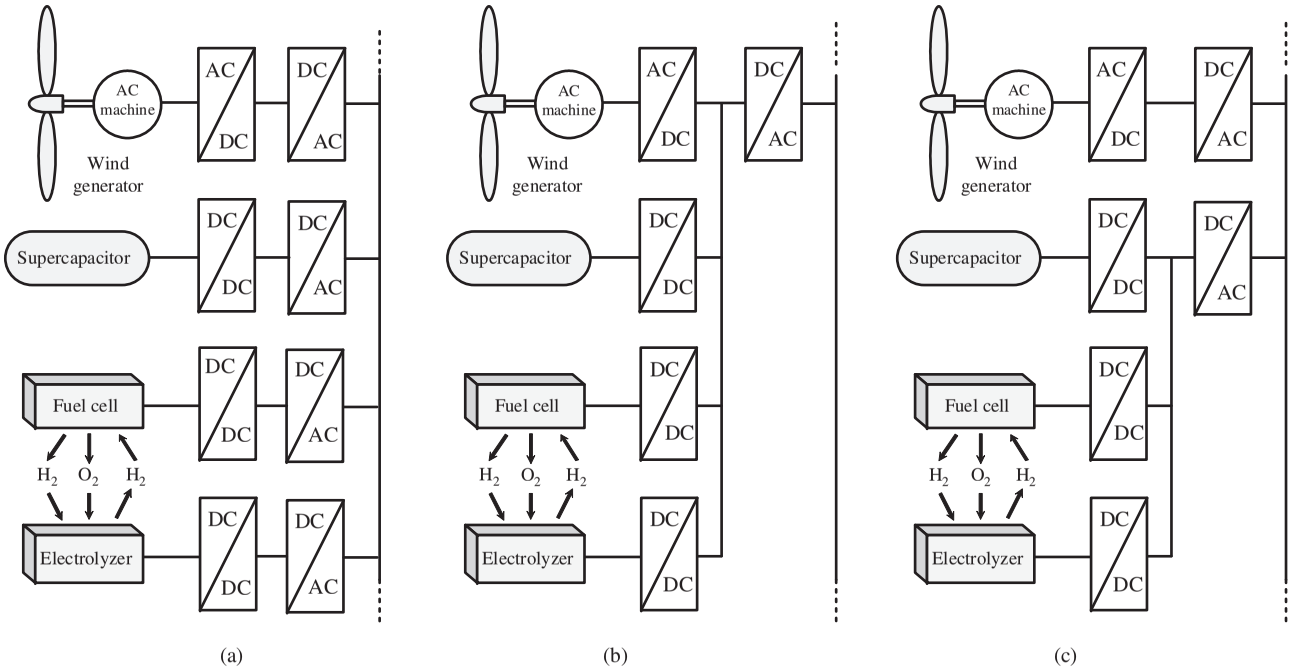

Figure 1.29 Structures of hybrid power systems for distributed generation.

meteorological conditions. Moreover, it becomes a considerable disturbance input for the grid power quality if many wind generators are used. ESSs can help to solve the fluctuation problem of the wind power and can ensure a good energy availability. However, additional control functions should be added to coordinate the different sources.

1.3.3.4 Wind Power Generators with Embedded Energy Storage Units in Hybrid Power Systems

The WPGs can work as distributed generators (DGs) together with other RESs and ESSs to perform an HPS. The DGs are usually smaller than 50 MW and are connected to the distribution network (directly or through an HPS), which has a low or medium operating voltage level.

The structures of HPSs can be classified into two categories: AC- and DC-coupled. In an AC-coupled HPS, all sources are connected to a main AC-bus before being connected to the grid (Fig. 1.29a) [13]. In AC-coupled structure, different sources can be located anywhere in the MG with a long distance from each other. However, the voltage and the frequency of the main AC bus should be well controlled in order to ensure the stability of the DG and the compatibility with the utility network.

In a *DC-coupled HPS*, all sources are connected to a main DC-bus before being connected to the grid through a main inverter (Fig. 1.29b). In a DC-coupled structure, the voltage and the frequency of the grid are independent from those of each source. The DC-coupled structure is flexible and expandable since the number and the type of the energy sources may be freely chosen. Even more, the grid frequency is independent from the sources through the use of the DC bus. The grid voltage is also independent from the DC-bus voltage and each source's voltage through the use of different power converters. So even if both control structure and power management are developed properly for a specified HPS, the number and type of the power sources do not alter the global control structure of the HPS and the main idea of the power management. However, not all HPSs can be classified into AC- or DC-coupled system, since it is possible to have both coupling methods (Fig. 1.29c) [14], then a mixed HPS is obtained. In this case, some advantages can be taken from both structures.

1.4 Grid-Connected PV Power

Large PV plants are being built all over the world, commonly having ratings up to 1 MW and reaching the level of 250 MW. These plants could be an alternative energy source for conventional ones and solving the energy dilemma of human community. However, the associated electronic systems, mainly inverters used for interfacing with the grid, have to solve some problems related to the operation in the electric distribution system. These systems should be reliable, robust,

and manageable. This section presents and discusses the most existing critical points in actual inverters, summarizing, explaining, and proposing approaches to solve or mitigate them.

Similar to the WPGs, the PV systems as SPGs are becoming economically viable, even without government subsidies. The PV system capacity is increasing continuously over the world reaching values of hundreds of megawatts; thus, making these plants would be a crucial part of future electric energy systems, MGs, and smart grids. These large/medium SPGs operate as distributed energy resources (DERs) mostly in rural areas where require enough surface for installing. They can be connected to radial distribution grids as shown in the example of Fig. 1.30.

1.4.1 Solar Power Generators with Embedded Energy Storage Systems

Electrical systems must ensure a balance between production and consumption at all times, while maintaining a satisfactory voltage. Grid reliability can be mainly ensured by having excessive capacity in the system with unidirectional flow from centrally dispatched large power plants to dispersed consumers. Dispatched production refers to sources of electricity that can be dispatched at the request of system operators. They are able to change their power production upon demand.

The large-scale development of intermittent PV sources causes large amount of variable power [15]. The RESs with intermittency decrease the reliability of a power system. As the percentage of intermittent generation capacity increases and becomes more significant, an additional uncertainty is appearing in the real-time management of the electrical system balance between demand and generation. This requires increasing amounts of conventional power reserve capacity (spinning reserve) that can be available immediately and of plants capable of providing ancillary services (e.g., frequency response and voltage control), which are required to manage the electrical power system securely [16]. However, an electrical generation system depending entirely on the RESs is not reliable because the availability of the RESs cannot be constantly ensured.

Because of the intermittency of PV power generation, the SPGs may not be used as a stable, reliable, and controllable power source and may not provide ancillary services such as conventional generators. One solution is to upgrade SPG with an embedded ESS and a local energy management system (LEMS) for the coordination of inner power flows. Storage technologies are varying and first it is essential to characterize the required need and complementary performances they must offer. Typically, an energy reserve must be provided to the electrical system and can be implemented by long-term energy storages. Moreover, the supply of power with fast dynamics is also mandatory to smooth the generated PV power, compensate the power gap, and absorb instantaneous high power peaks. At the present state of the art, a high energy storage unit

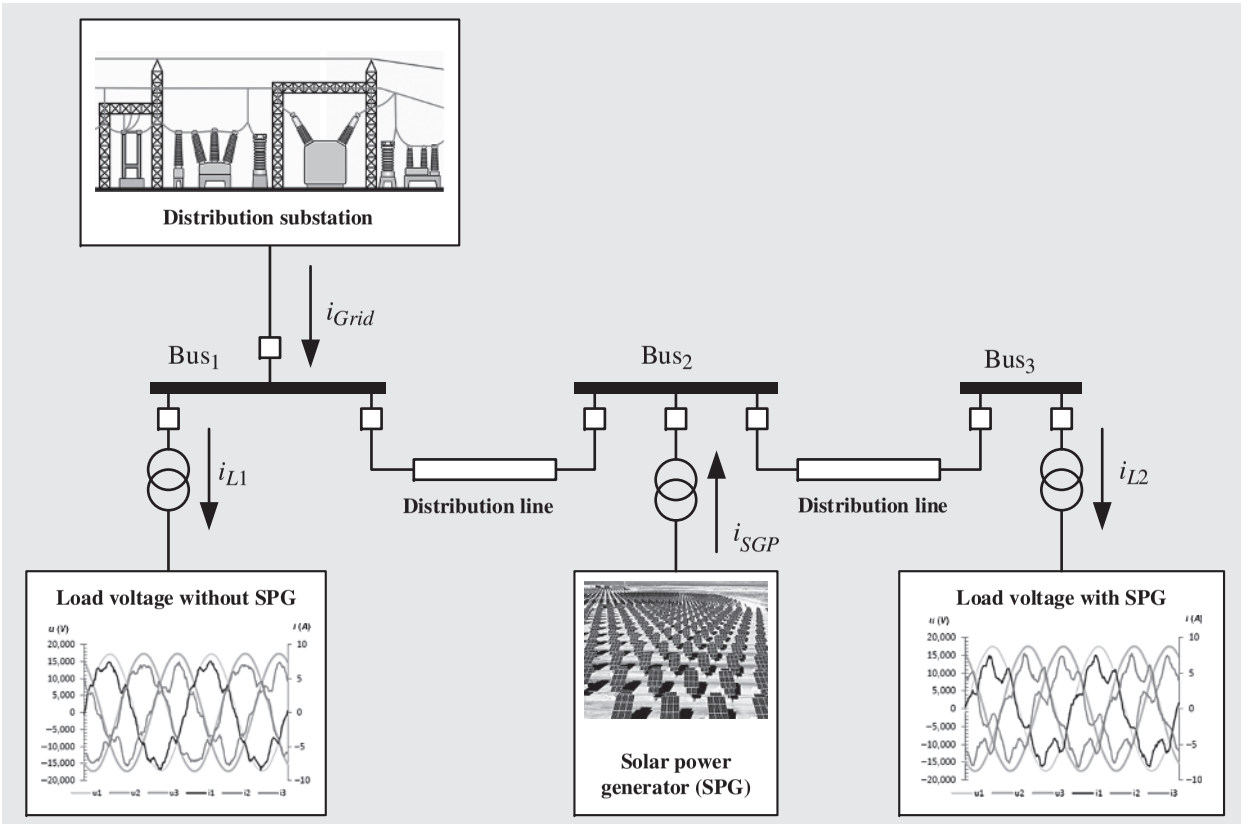

Figure 1.30 A distribution grid example with connected SPGs.

delivering high power with fast dynamics in a reduced volume does not exist and a mix of storage technologies has to be considered. Lead acid batteries for long-term energy storage device and ultracapacitors for fast dynamic power regulation are today realistic and economic choices, but other technologies can also be considered, for example, fuel cells, REDOX batteries, and flywheels.

Storage devices can be used to store or release electrical power such as an energy buffer. Therefore, they can help to solve problems due to renewable energies' intermittent availabilities and fast transients. The SPGs combined with the ESSs perform an HPS, which can be considered as an active PV generator for the grid since it can supply ancillary services as conventional generators. Moreover, it can be dispatched and then provide a power reference that is demanded by the grid operator [17].

A general structure that has been widely used in isolated power systems for integrating the ESSs is based on the direct connection of a battery bank to the DC-bus of the grid-connected inverter. A PV controller is used to extract the maximum power from PV panels and send it to the battery bank. However, the stochastic nature of PV and demand powers lead to fast charge/discharge actions of batteries and a fast battery aging.

To enable a more efficient use of batteries, AC- and DC-coupled power electronic converters can be considered in order to have control abilities of the exchanged powers with the batteries, thanks to the development of power electronics. In an AC-coupled HPS structure, all sources are connected to the main AC network (Fig. 1.31a) [17]. A communication network is required to implement the coordination of this set. In a DC-coupled HPS, all sources are connected to a common inner DC-bus before being connected to the grid through a main inverter (Fig. 1.31b) [18]. One advantage is that the battery bank is connected to the DC-bus via a DC/DC converter, which can be used to implement an optimized charge/discharge operation mode. The second advantage is that a supercapacitor bank is added and is also connected to the DC bus via another DC/DC converter. Hence, a fast power compensation can be performed. The PV array is connected to the DC bus via a PV converter. Similar to the WPGs (Fig. 1.29), apart from these two coupling structures, a mixed structure can be also used (Fig. 1.31c) with some advantages of both DC- and AC-coupled structures.

1.4.2 Solar Energy Conversion System: Modeling, Control, and Analysis

The interest for a PV-based hybrid active generator and the need for grid operator to get more dispatched DGs have been already justified. As mentioned, in order to have a local energy reserve and to filter fast PV power fluctuations, ESS is used to build a PV/ESS HPS in a DC-coupled structure.

The power flows between the different sources must be controlled in order to supply the real and reactive power required by the grid operator

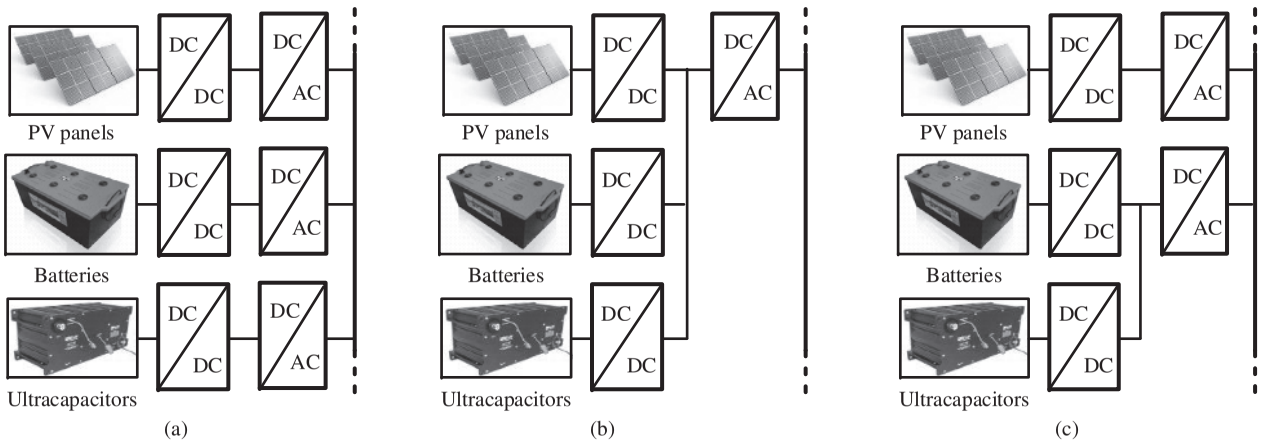

Figure 1.31 Various structures of HPSs: (a) AC-coupled, (b) DC-coupled, and (c) mixed structure.

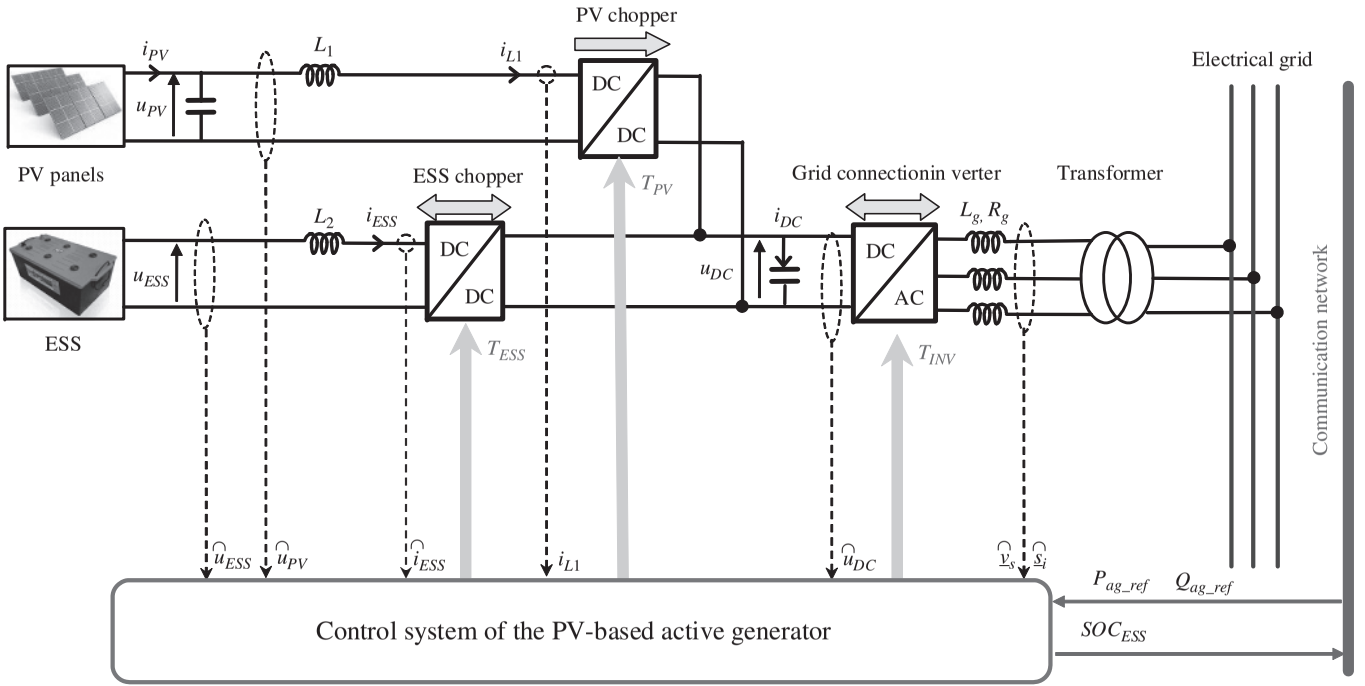

Figure 1.32 Grid-connected PV-based active generator with the control system.

(P_{ag_ref}, Q_{ag_ref}). This is performed by the control of different power electronic converters, which must be then coordinated (Fig. 1.32). Different control strategies have been presented to design the energy management of HPSs and for various applications.

In this section, first the entire PV-based active generator is modeled and then a hierarchical control structure is used and the design of the control system, including the power balancing and energy management strategies are detailed. Similar to the WPGs modeling method, in order to design the control system of the PV active generator, the model of the entire system has to be analyzed. For the modeling of the PV-based active generator, all the modulated values can be replaced by their average values during the modulation period. So each power electronic converter can be replaced by an equivalent double modulated generator (Fig. 1.33).

The equivalent electrical diagram with the equivalent average modeling of power electronic converters makes appear three parts corresponding to the PV conversion system: the ESS, the grid connection, and the DC bus. The three power converters are used to introduce control inputs for each power conversion system, in order to control the power generated by the PV panels, to maintain a constant DC-bus voltage, to supply the required power exchange with the grid, and to ensure the power buffering of each energy storage unit.

1.4.2.1 PV Power Conversion System

In the PV power conversion model, the PV panels are usually considered as a current source (i_{PV}) and it must be supplied by a voltage (u_{PV}) [19]. The voltage comes from a filter (C_1, L_1), which is fed by the modulated voltage (Fig. 1.34).

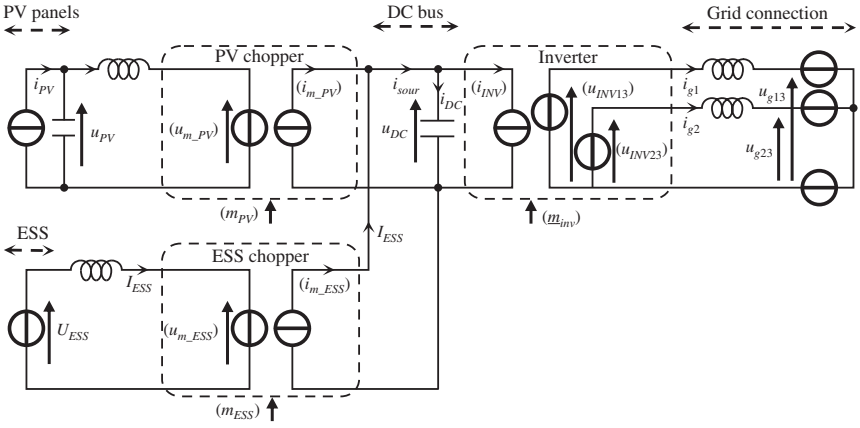

Figure 1.33 Equivalent electrical diagram of the PV-based active generator.

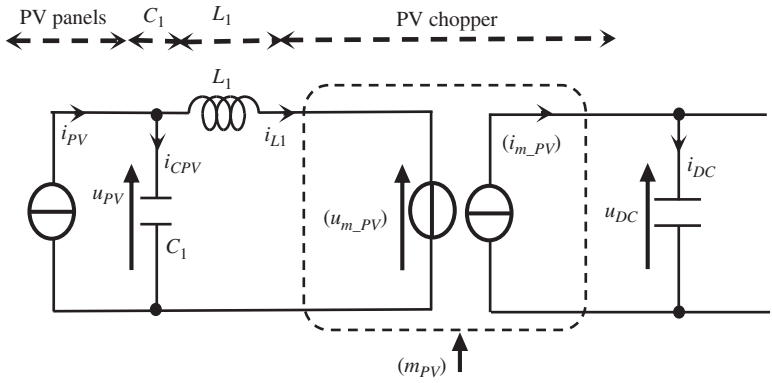

Figure 1.34 Equivalent electrical diagram of PV power conversion system.

The choke is also modeled as a current source (i_{L1}). This current depends on the PV voltage and the modulated voltage of the chopper output (u_{m_PV}):

$$\frac{di_{L1}}{dt} = \frac{1}{L_1}(u_{m\_PV}(t) - u_{PV}(t)) \tag{1.35}$$

Losses in the filter and the capacitor are neglected. The capacitor (C_1) can stabilize the voltage (u_{PV}) across the terminals of the PV panels. This capacitor can be modeled by using the PV current (i_{PV}) and the filtered current (i_{L1}):

$$\begin{cases} \dfrac{du_{PV}}{dt} = \dfrac{1}{C_1} i_{CPV}(t) \\ i_{CPV}(t) = i_{PV}(t) - i_{L1}(t) \end{cases} \tag{1.36}$$

i_{CPV} is the injected current in capacitor. The mean value of the terminal voltage of the chopper (u_{m_PV}) is obtained from the DC voltage (u_{DC}) and the duty cycle ratio ($m_{\_PV}$):

$$\begin{cases} \langle u_{m\_PV} \rangle = m_{PV} \cdot u_{DC}(t) \\ \langle i_{m\_PV} \rangle = m_{PV} \cdot i_{L1}(t) \end{cases} \tag{1.37}$$

It is noteworthy that the notation $\langle x \rangle$ means "the average values of the instantaneous electrical quantities" $x(t)$, but since here all quantities are in mean values, the notation $\langle x \rangle$ will not be used later.

1.4.2.2 Energy Storage System

In the models of ESSs, an ESS is usually considered as a voltage source (u_{ESS}), which is connected to a choke filter (L_2) (Fig. 1.35).

By neglecting losses in the filter, the dynamic equation of the filtered current (i_{ESS}) is expressed with the ESS voltage (u_{ESS}) and the modulated

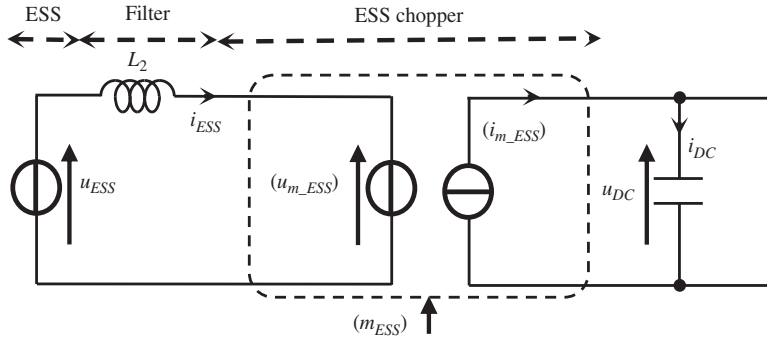

Figure 1.35 Equivalent electrical diagram of the batteries energy storage system.

voltage (u_{m_ESS}):

$$\frac{di_{ESS}}{dt} = \frac{1}{L_2} \cdot (u_{ESS}(t) - u_{m\_ESS}(t)) \tag{1.38}$$

where L_2 is the inductor of the filter.

The mean value of the terminal voltage of the ESS chopper (u_{m_ESS}) is obtained from the DC voltage and the duty cycle ratio (m_{ESS}):

$$\begin{cases} u_{m\_ESS} = m_{ESS} \cdot u_{DC}(t) \\ i_{m\_ESS} = m_{ESS} \cdot i_{ESS}(t) \end{cases} \tag{1.39}$$

In the same way, the filtered current (i_{ESS}) is modulated by the chopper, and then this modulated current (i_{m_ESS}) is injected into the common DC bus. The average value of the output current (i_{m_ESS}) of the chopper is equal to the ESS current (i_{ESS}) multiplied by the duty cycle ratio (m_{ESS}).

1.4.2.3 Grid Connection

A three-phase inverter within a choke as filter is used for the grid connection. Hence, an equivalent mean modeling of this three-phase inverter is sufficient for representing fundamental components of voltage/current (Fig. 1.36) as dependent phase-to-phase voltage sources (u_{INV_13} and u_{INV_23}) with the DC-bus voltage (u_{DC}) through modulation indexes (m_{INV_13} and m_{INV_23}) and a dependent current source (i_{INV}) with AC currents through the same modulation indexes.

Then mean values of modulated phase-to-phase voltages and of the average currents are expressed as

$$\begin{cases} u_{INV\_13} = m_{INV\_13} \cdot u_{DC} \\ u_{INV\_23} = m_{INV\_23} \cdot u_{DC} \end{cases} \tag{1.40}$$

$$\langle i_{INV} \rangle = m_{INV\_13} \cdot i_{g1} + m_{INV\_23} \cdot i_{g2} \tag{1.41}$$

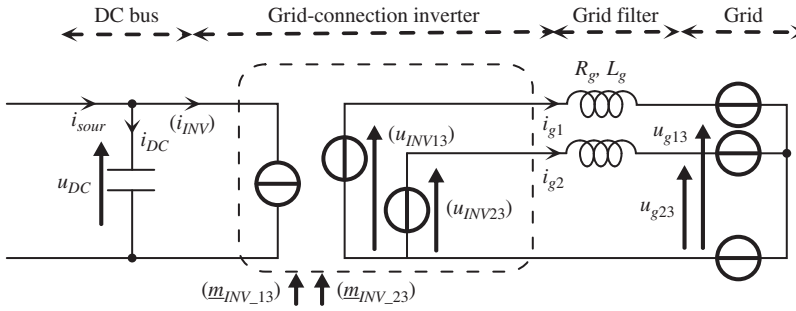

Figure 1.36 Electrical diagram of the grid connection.

By assuming that grid voltages are balanced, line voltages are obtained through

$$\begin{cases} v_{INV1} = \frac{2}{3} \cdot u_{INV\_13} - \frac{1}{3} \cdot u_{INV\_23} \\ v_{INV2} = -\frac{1}{3} \cdot u_{INV\_13} + \frac{2}{3} \cdot u_{INV\_23} \end{cases} \tag{1.42}$$

The filter currents are deduced from the following differential equations:

$$\begin{cases} \dfrac{di_{g1}}{dt} = \dfrac{1}{L_g} \left(v_{INV1} - R_g \cdot i_{g1} - v_{g1} \right) \\ \dfrac{di_{g2}}{dt} = \dfrac{1}{L_g} \left(v_{INV2} - R_g \cdot i_{g2} - v_{g2} \right) \end{cases} \tag{1.43}$$

Three-phase inverter voltages, grid voltages, currents, and duty cycles can be expressed as vectors, respectively, by

$$\underline{v_{INV}} = \begin{bmatrix} v_{INV1} \\ v_{INV2} \\ v_{INV3} \end{bmatrix}, \quad \underline{v_g} = \begin{bmatrix} v_{g1} \\ v_{g2} \\ v_{g3} \end{bmatrix}, \quad \underline{i_g} = \begin{bmatrix} i_{g1} \\ i_{g2} \\ i_{g3} \end{bmatrix}, \quad \underline{m_{INV}} = \begin{bmatrix} m_{INV\_13} \\ m_{INV\_23} \end{bmatrix} \tag{1.44}$$

1.4.2.4 DC Bus

In this hybrid generating system, three energy sources (PV panels, ESS, and the electrical grid) are all connected to the common DC bus via different power electronic converters (Fig. 1.33). So according to this DC-coupling, the capacitor current of the DC bus (i_{DC}) is expressed as

$$i_{sour}(t) = i_{ESS}(t) + i_{m\_PV}(t) \tag{1.45}$$

$$i_{DC}(t) = i_{sour}(t) - i_{INV}(t) \tag{1.46}$$

where i_{m_PV} is the modulated current from the PV chopper, i_{m_ESS} is the modulated current from the ESS chopper, and i_{INV} is the modulated current from the grid inverter.

DC-bus voltage is expressed as

$$\frac{du_{DC}}{dt} = \frac{1}{C_{DC}} i_{DC}(t) \tag{1.47}$$

The C_{DC} is the capacitor of the DC bus.

1.4.2.5 Modeling of the Entire PV Energy Conversion System

By combining the all mentioned sources' power conversion system models, which is discussed in the previous sections, the block diagram of the entire active PV generator can be obtained as shown in Fig. 1.37. Three action paths appear from the control inputs of the three power converters to the different electrical quantities (u_{PV}, i_{ESS}, $\underline{i}_g$): from the PV chopper (m_{PV}) to the PV panels terminal voltage (u_{PV}) in yellow, from the ESS chopper (m_{ESS}) to the batteries current (i_{BAT}) in green, and finally from the grid connection three-phase inverter ($\underline{m}_{INV}$) to the line currents ($\underline{i}_g$) in blue.

1.4.2.6 Hierarchical Control Structure

Like WPG hierarchical system (Fig. 1.11), a hierarchical structure of the control system is proposed for this active PV generator. The structure of this hierarchical control system includes four levels (Fig. 1.38). Each one has precise control tasks depending on its hierarchical position: SCU, ACU, PCU, and MCU.

The MCU decides the operating mode for the whole hybrid generator according to the availability of the PV production, the states of each storage unit and the actual power demand from the grid. The PCU calculates the power reference for each source according to the sensed values and the selected operating mode from the MCU. The ACU applies the control algorithm to meet the current or voltage references. The SCU level implements the modulation technique to each converter and generates the semiconductor signals ({−5, +15}) to apply wished ideal states ({0, 1}).

In the studied active PV generator, three sources are considered: the PV panels (PV), the ESS, and the grid connection. Three power electronic converters are used to regulate the power exchanges among them. So in the control system, three SCUs and three ACUs are used for the control of the three sources, a common PCU and a common MCU are used for the power dispatching among the different sources, the real-time power balancing and the long-term energy management of the entire active generator (Fig. 1.38).

In the SCU of each power electronic converter, the IGBT and PWM techniques are used to control the switches. The control algorithms in the ACU level should be presented in order to highlight the physical quantities, which can be used for the power flow control among the different energy sources.

1.4.2.6.1 Automatic Control Unit The task of the ACU is to calculate duty cycles for each SCU in order to set dynamical quantities equal to their references (current and voltage), which are coming from the PCU.

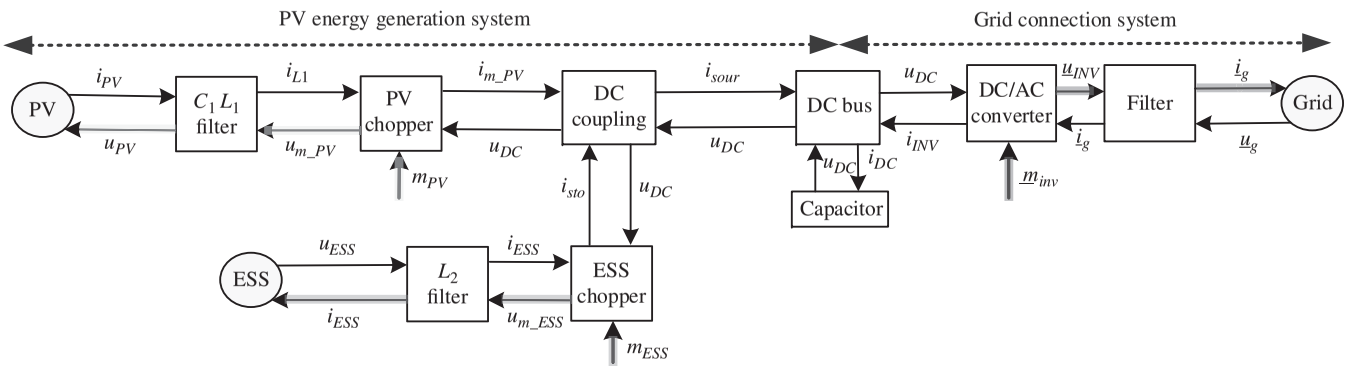

Figure 1.37 The block diagram of the PV active generator.

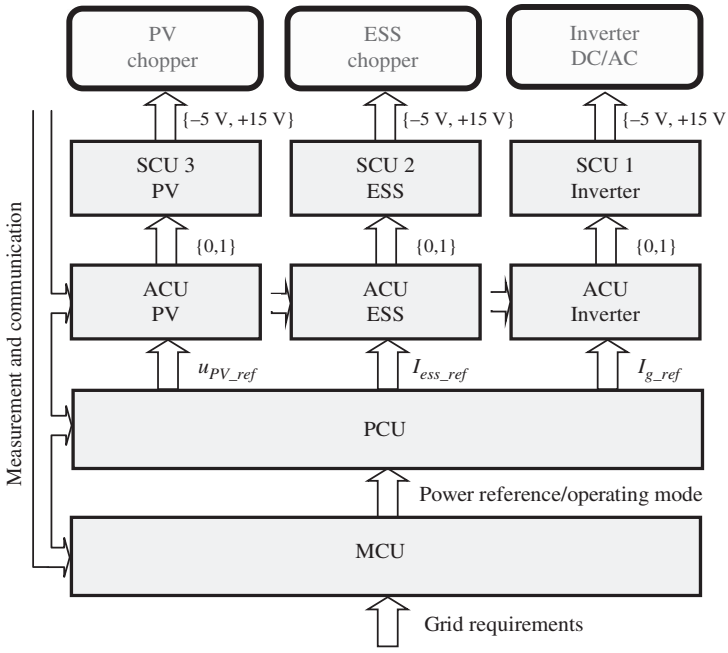

Figure 1.38 Hierarchical control structure for the active PV generator.

PV Controller The ACU of the PV power conversion system must regulate the terminal voltage across the PV panels in order to implement an MPPT strategy or a power limitation (PL) strategy. The variation of this voltage modifies the generated PV power (Fig. 1.39).

The PV power conversion system provides an action chain from the duty cycle ratio (m_{PV}) and pointing to the PV terminal voltage (u_{PV}). According to the inversion rules of the CSU, the automatic control system is achieved by

- a closed-loop control of the filtered current (i_{L1}) with a simple controller (K_1),

$$u_{m\_PV\_ref} = K_1(i_{L1\_ref} - i_{L1\_mes}) + u_{PV\_mes} \tag{1.48}$$

- a closed-loop control of the terminal voltage (u_{PV}) with a simple controller (K_2),

$$i_{L1\_ref} = K_2(u_{PV\_ref} - u_{PV\_mes}) + i_{PV\_mes} \tag{1.49}$$

- a converter control for the calculation of the duty cycle, which will be sent to the SCU:

$$m_{PV\_reg} = \frac{u_{m\_PV\_ref}}{u_{DC\_mes}} \tag{1.50}$$

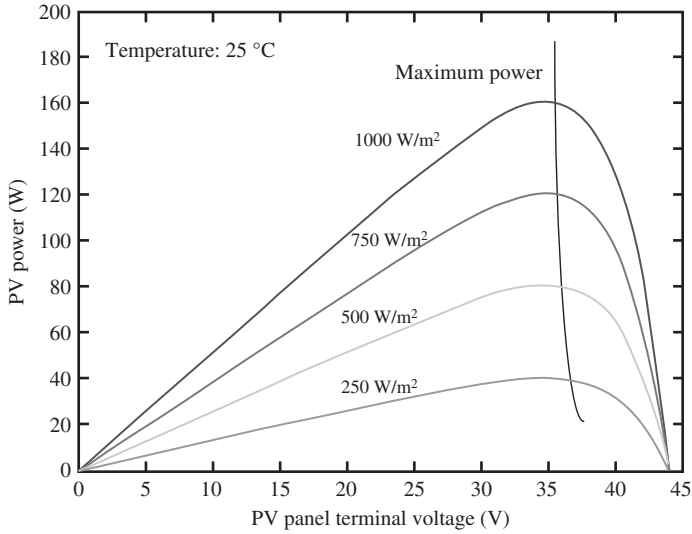

Figure 1.39 Power characteristics of one PV module.

EES Controller From the ESS, an action chain from the duty cycle ratio (m_{ESS}) and pointing to the ESS current (i_{ESS}) can be considered. A control chain is obtained by inversing this action chain. The inversion rules of the CSU yields two control functions:

- A closed-loop control of the current with a controller (K_3)

$$u_{m\_ESS\_ref} = K_3(i_{ESS\_ref} - i_{ESS\_mes}) \tag{1.51}$$

- A converter controller to calculate the duty cycle ratio, which will be sent to the SCU:

$$m_{ESS\_reg} = \frac{u_{m\_ESS\_ref}}{u_{DC\_mes}} \tag{1.52}$$

Grid Connection Control The block diagram of the grid connection system modeling makes appear a path in blue from the control inputs ($\underline{m}_{inv}$) of the inverter to the line currents ($\underline{i}_g$). The control scheme of the grid connection system is obtained by inverting this path. It involves calculating the reference of the inverter's duty ratios ($\underline{m}_{inv\_ref}$) according to the line currents' references ($\underline{i}_{g\_ref}$). The objective of the grid connection control is to regulate the delivered active power and reactive power to the grid. The grid is a voltage source ($\underline{u}_{grid}$), so the line current should be controlled in order to regulate the exchanged power with the grid. Hence, the delivered power control is based on the grid current control. According to the inversion rules of the CSU, the automatic

control system is achieved by an inverter controller and a closed-loop control of currents.

For the design of controllers, a Park transform is used. The voltages and currents in the three-phase frame (a,b,c) can be transformed to two voltages and two currents in the two-phase rotating frame (d,q) with synchronization with the first line voltage:

$$\begin{cases} \underline{v_{inv\_dq}} = P(\theta)\underline{v_{INV}} \\ \underline{v_{g\_dq}} = P(\theta)\underline{v_g} \\ \underline{i_{g\_dq}} = P(\theta)\underline{i_g} \end{cases} \tag{1.53}$$

$P(\theta)$ is the matrix of the Park transformation.

$$P(\theta) = \frac{2}{3}\begin{bmatrix} \cos\theta & \cos\left(\theta - \frac{2\pi}{3}\right) & \cos\left(\theta + \frac{2\pi}{3}\right) \\ \sin\theta & \sin\left(\theta - \frac{2\pi}{3}\right) & \sin\left(\theta + \frac{2\pi}{3}\right) \\ \frac{1}{2} & \frac{1}{2} & \frac{1}{2} \end{bmatrix} \tag{1.54}$$

Hence in this frame, filter current equations are expressed as

$$\begin{cases} \dfrac{di_{g\_d}}{dt} = \dfrac{1}{L}\left(v_{inv\_d} - v_{g\_d} - R_g i_{g\_d} - L_g \cdot \omega_s \cdot \ i_{g\_q}\right) \\ \dfrac{di_{g\_q}}{dt} = \dfrac{1}{L}\left(v_{inv\_q} - v_{g\_q} - R_g i_{g\_q} + L_g \cdot \omega_s \cdot \ i_{g\_d}\right) \end{cases} \tag{1.55}$$

where $\omega_s = 2\pi f$ and f is the grid frequency.

Therefore, similar to the block diagram shown in Fig. 1.16, the control of these currents is organized in three parts: proportional–integral (PI) control, grid voltage compensation, and current decoupling. The modulated voltage references of the inverter outputs can be expressed as

$$\begin{cases} v_{inv\_d\_ref} = PI_1(i_{g\_d\_ref} - i_{g\_d\_mes}) + v_{g\_d\_mes} - L_g \cdot \omega_s \cdot \ i_{g\_q\_mes} \\ v_{inv\_q\_ref} = PI_2(i_{g\_q\_ref} - i_{g\_q\_mes}) + v_{g\_q\_mes} + L_g \cdot \omega_s \cdot \ i_{g\_d\_mes} \end{cases} \tag{1.56}$$

with two current PI correctors (PI_1, PI_2).

The obtained voltage references in the dq frame can be transformed to the three voltage references in the abc frame with an inverse Park transformation:

$$\underline{v_{inv\_ref}} = P^{-1}(\theta)\underline{v_{inv\_dq\_ref}} \tag{1.57}$$

Phase-to-phase voltages are obtained with the following equations:

$$\begin{cases} u_{inv13\_ref} = v_{INV1\_ref} - v_{inv3\_ref} \\ u_{inv23\_ref} = v_{INV2\_ref} - v_{inv3\_ref} \end{cases} \tag{1.58}$$

Mean values of the modulation functions are calculated by using the inverse equation (1.40):

$$m_{inv13\_reg} = \frac{u_{inv13\_ref}}{u_{DC\_mes}}, \quad m_{INV23\_reg} = \frac{u_{inv23\_ref}}{u_{DC\_mes}} \tag{1.59}$$

DC Bus Control The decomposition into the different subsystems relies on the assumption that the DC-bus voltage (u_{DC}) is constant. The control scheme of the DC bus is obtained by inverting the block diagram of the system modeling (similar to Fig. 1.17) and requires a closed-loop control of the DC-bus voltage (u_{DC}) with a PI corrector (PI):

$$i_{DC\_ref} = PI(u_{DC\_ref} - u_{DC\_mes}) \tag{1.60}$$

The current flowing through the capacitor of the DC bus (i_{DC}) can be expressed as

$$i_{DC} = i_{m\_PV} + i_{m\_ESS} - i_{inv} \tag{1.61}$$

Thus, the regulation of the current in the capacitor can be achieved by controlling the currents of each source (PV panels and ESS) corresponding to the power control of each source.

Control of the Entire PV Energy Conversion System The global control scheme of the entire active PV generator can be obtained by combining all control schemes, which have been explained in the previous parts, as shown in Fig. 1.40. A block diagram of all control functions inside the ACU is also presented in Fig. 1.41. Four references (i_{DC_ref}, i_{g_ref}, u_{PV_ref}, and i_{ESS_ref}) must be set to interface the automatic control level with the PCL.

1.4.2.6.2 Power Control Unit The PCU is divided into two levels: the PCL and the PSL. The PCL involves calculating the reference quantities (i_{g_ref}, u_{PV_ref}, i_{ESS_ref}) from power references. The PSL coordinates the power flow exchanges among the different energy sources with different power balancing strategies.

To implement the power control, the inner power flow of the active generator has to be calculated. In order to focus on the power exchanges with the different sources around the DC bus, the instantaneously exchanged power with the choke, the losses in the filters and the losses in the power converters are neglected. Only the sources' powers and the exchanged power with the DC-bus capacitor are taken into account here (Fig. 1.42). Powers in the DC part are easily calculated by multiplying DC currents and DC voltages (Table 1.2). All the variables with hat symbol are the sensed variables. The expressions of the powers are inverted to obtain the control equations (Fig. 1.42).

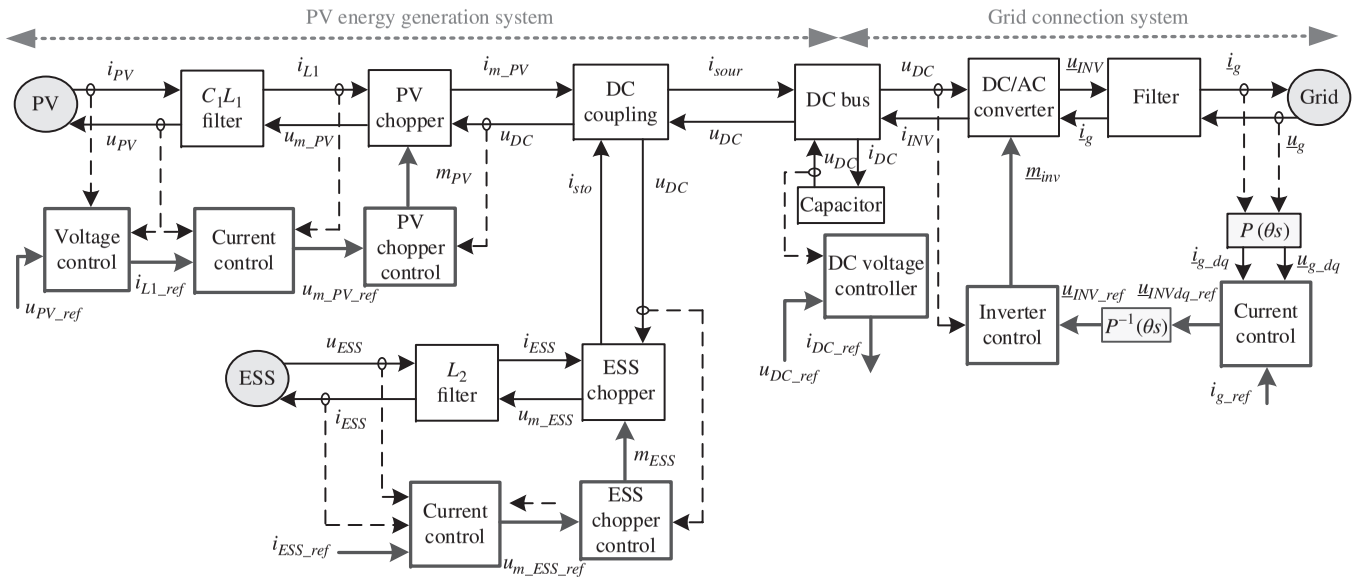

Figure 1.40 Block diagram of a grid-connected PV system with control loops.

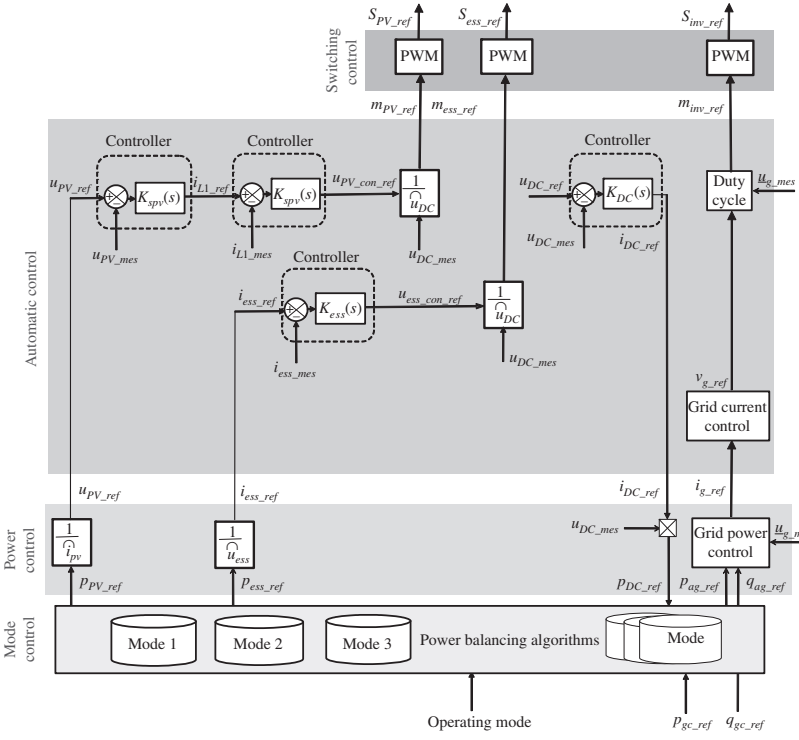

Figure 1.41 Block diagram of the automatic control units for the active PV generator.

Table 1.2 Power calculation and power control algorithms for the active PV generator.

Energy source	Power calculation	Power control
DC-bus capacitor	$p_{DC} = u_{DC} i_{DC}$ (iv)	$p_{DC\_ref} = \widehat{u}_{DC} i_{DC\_ref}$ (iv_c)
Grid connection	$\begin{cases} p_{ag} = u_{g13} \cdot i_{g1} + u_{g23} \cdot i_{g2} \\ q_{ag} = \sqrt{3}(u_{g13} \cdot i_{g1} - u_{g23} \cdot i_{g2}) \end{cases}$ (v)	$\begin{cases} i_{g1\_ref} = \dfrac{(2\widehat{u}_{13} - \widehat{u}_{23}) p_{ag\_ref} + \sqrt{3}\widehat{u}_{23} q_{ag\_ref}}{2\widehat{u}_{13}^2 - 2\widehat{u}_{13}\widehat{u}_{23} + 2\widehat{u}_{23}^2} \\ i_{g2\_ref} = \dfrac{(2\widehat{u}_{23} - \widehat{u}_{13}) p_{ag\_ref} - \sqrt{3}\widehat{u}_{13} q_{ag\_ref}}{2\widehat{u}_{13}^2 - 2\widehat{u}_{13}\widehat{u}_{23} + 2\widehat{u}_{23}^2} \end{cases}$ (v_c)
PV panels	$p_{PV} = u_{PV} i_{PV}$ (vi)	$u_{PV\_ref} = \dfrac{1}{\widehat{i}_{PV}} p_{PV\_ref}$ (vi_c)
ESS	$p_{ESS} = i_{ESS} u_{ESS}$ (vii)	$i_{ESS\_ref} = \dfrac{1}{\widehat{u}_{ESS}} p_{ESS\_ref}$ (vii_c)

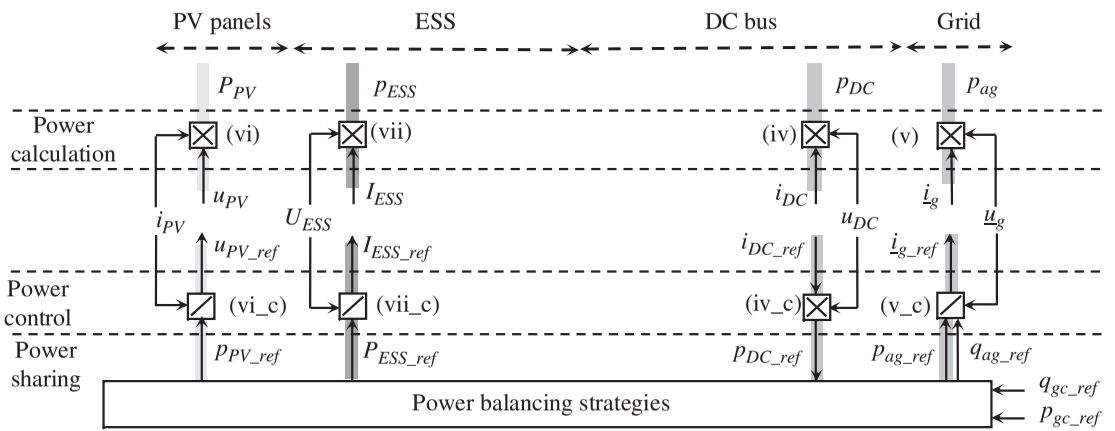

Figure 1.42 Power modeling and control.

Power control of PV panels: A reference value for the PV power can be set by calculating the PV voltage reference (u_{PV_ref}) with the sensed PV current:

$$u_{PV\_ref} = \frac{p_{PV\_ref}}{i_{PV\_mes}} \tag{1.62}$$

Power control of storage units: For the storage systems, the powers are calculated by multiplying currents with the voltages ((vii) in Table 1.2). The current references are given by dividing corresponding power references with the sensed voltages.

Power control of the grid connection: The powers, which are exchanged with the grid, can be calculated through the "two-wattmeter" method ((v) in Table 1.2). According to the grid power reference and the measured phase-to-phase voltages of the grid, the current references for the inverter can be deduced by inverting this equation ((v_c) in Table 1.2).

Power control of the DC bus: The output of the DC-bus voltage control loop is the current reference (i_{DC_ref}) of the DC-bus capacitor, and its product with the measured DC-bus voltage gives the power reference (p_{DC_ref}) for the DC-bus voltage regulation (iv_c). This regulation power for the DC-bus voltage control can be satisfied by the difference between the sources power and the grid power.

The DC bus directly leads to the stability of the generator. All power exchanges are performed via the DC-bus and have an impact on the DC-bus voltage (u_{DC}):

$$C_{DC}u_{DC}\frac{du_{DC}}{dt} = \frac{dE_{DC}}{dt} = p_{DC} = p_{sour} - p_{ag} = p_{ESS} - p_{ag} \tag{1.63}$$

where E_{DC} is the energy stored in the DC-bus capacitor; p_{DC} is the resulted power into the DC-bus capacitor; p_{PV} is the power injected into the DC bus from the PV generator; p_{ESS} is the power exchanged between the EES and the DC bus; p_{ag} is the power extracted from the DC bus into the grid; and p_{sour} is the total power from the sources. So to get a constant DC-bus voltage, the instantaneous powers must be balanced. For different studied modes, the power flow must be then modeled in order to be controlled in a second step.

Power sharing: The PSL is used to implement the power balancing strategies in order to coordinate the various sources in the HPS. The power references for each source are set according to different power control strategies, which are specific to different operating modes. Operating modes are defined according to the various conditions (the power demand from the grid, the availability of the PV power, the state of the energy storage units, etc.). In order to set the power reference of each source, the power flow between each source should be determined and balanced. So a modeling of the power flow in the active generator for each mode is necessary.

1.4.3 Experimental Results

Figure 1.43a outlines the used DC-coupled active PV generator as an HPS prototype test system. The grid connection is performed by a three-phase inverter. Chokes and capacitors are used to filter the modulated electrical waveforms. Here, the EES includes two sets of lead-acid batteries (48 V, 106 Ah) and ultracapacitors (48 V, 112 kW min). A DC current source is used for simulating the PV panels. The control system is implemented into a DSP card. Figure 1.43b shows the experimental laboratory systems.

In order to ensure an optimal operation and coordination, an LEMS of the active PV generator must calculate and send control signals to each power electronic converter in order to enable production of power demand for the grid operator, management of renewable energy intermittency, management of storage state of charges (SOC), power system protection, and provision of grid ancillary services.

A hierarchical control structure for the given HPS system (Fig. 1.38) similar to the one in Fig. 1.41 can be considered. The SCU implements the modulation technique to each converter and generates the switching signals. The ACU performs control algorithms in order to meet the current or voltage references. The PCU calculates these references according to the power references from the MCU and measured values. The MCU decides the operating mode for the whole hybrid generator according to the availability of the PV production, the state of each storage unit, and the actual power demand from the grid.

The power reference for the PV generator, $p_{PV\_ref}(t)$, is classically calculated from a maximum PV power tracking algorithm. The inner power balancing shows that powers from the PV, $p_{PV}(t)$, the battery, $p_{BAT}(t)$, the ultracapacitor, $p_{UC}(t)$ must be decreased by the required power to regulate the DC bus, $p_{DC}(t)$, and constitutes the total generated power [21]:

$$p_{ag}(t) = p_{BAT}(t) + p_{UC}(t) + p_{PV}(t) - p_{DC}(t) \tag{1.64}$$

There are two operation strategies for an active PV generation system: grid-following strategy (GFS) and source supplying strategy (SSS). The GFS and SSS are conceptually shown in Fig. 1.44a,b, respectively. Using the GFS, the reference for the power (generated by the inverter) is deduced using the measured power and contributes to the regulation of the DC bus:

$$p_{ag\_ref}(t) = \widehat{p}_{BAT}(t) + \widehat{p}_{UC}(t) + \widehat{p}_{PV}(t) - p_{DC\_ref}(t) \tag{1.65}$$

Then the required power reference from the grid operator is provided by the storage units taking into account the available PV power.

$$p_{sto\_ref}(t) = p_{gc\_ref}(t) - \widehat{p}_{PV}(t) \tag{1.66}$$

A simple method to dispatch the power between batteries and ultracapacitors can be realized using a slope-limited low-pass filter [22]. Ultracapacitors are controlled to supply the required transient power from storage units.

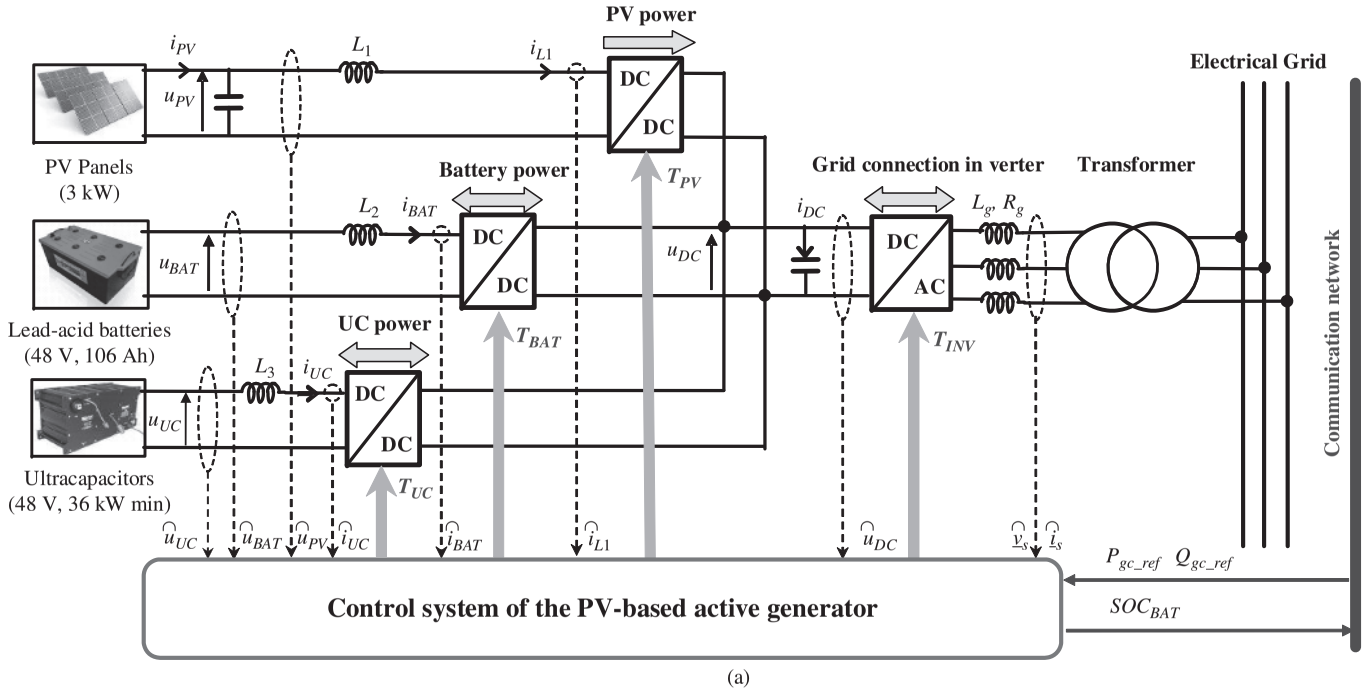

Figure 1.43 The grid-connected active PV generator (HPG) test system: (a) system configuration and (b) experimental units.

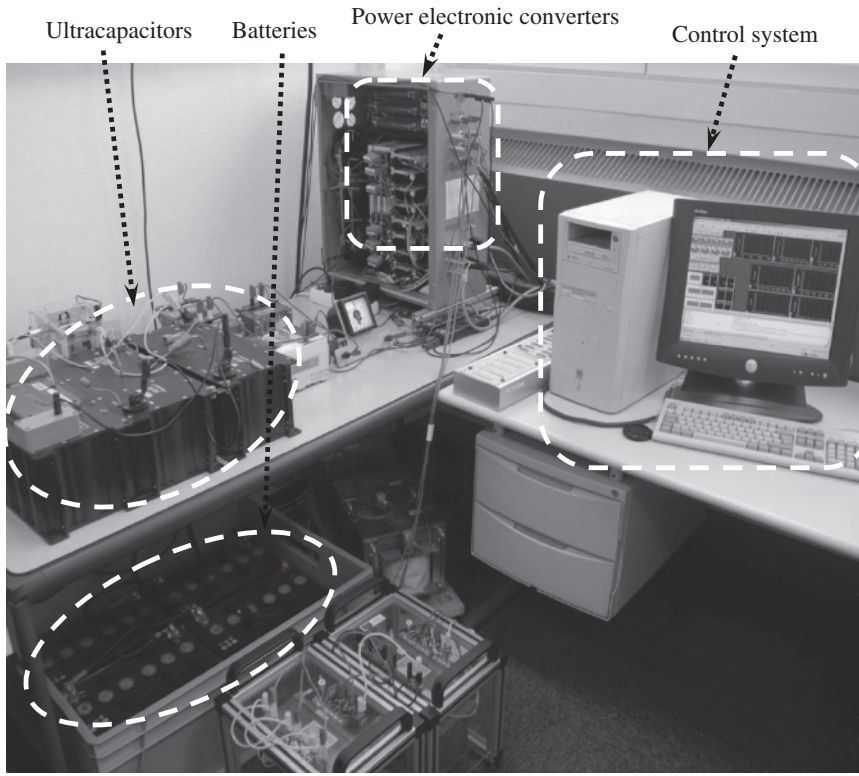

(b)

Figure 1.43 (*Continued*)

Using the SSS, the power from the storage units is adjusted according to the sensed PV power to regulate the DC bus. The required power reference is fixed by the grid operator, which can be directly provided by the inverter.

With both strategies, the PV generator can be dispatched by the grid operator since it is now able to deliver the prescribed active and reactive powers ($p_{gc\_ref}(t)$, $q_{gc\_ref}(t)$), but only the SSS is able to work without a connection to the grid because the DC bus is regulated by the inner power. This strategy is preferred since autonomous/isolated operation is possible and may be used to store PV energy without grid connection. Another advantage is the possibility to stay connected in case of undervoltage grid because the DC-bus voltage is autonomously regulated by inner sources (PV panels and storage units). Hence, in this situation, the real and reactive power generation is possible to help the electric network [23].

Using the mentioned strategy, a test scenario is performed in the daytime having a step change in the injected reference power into the grid (p_{gc_ref}). The

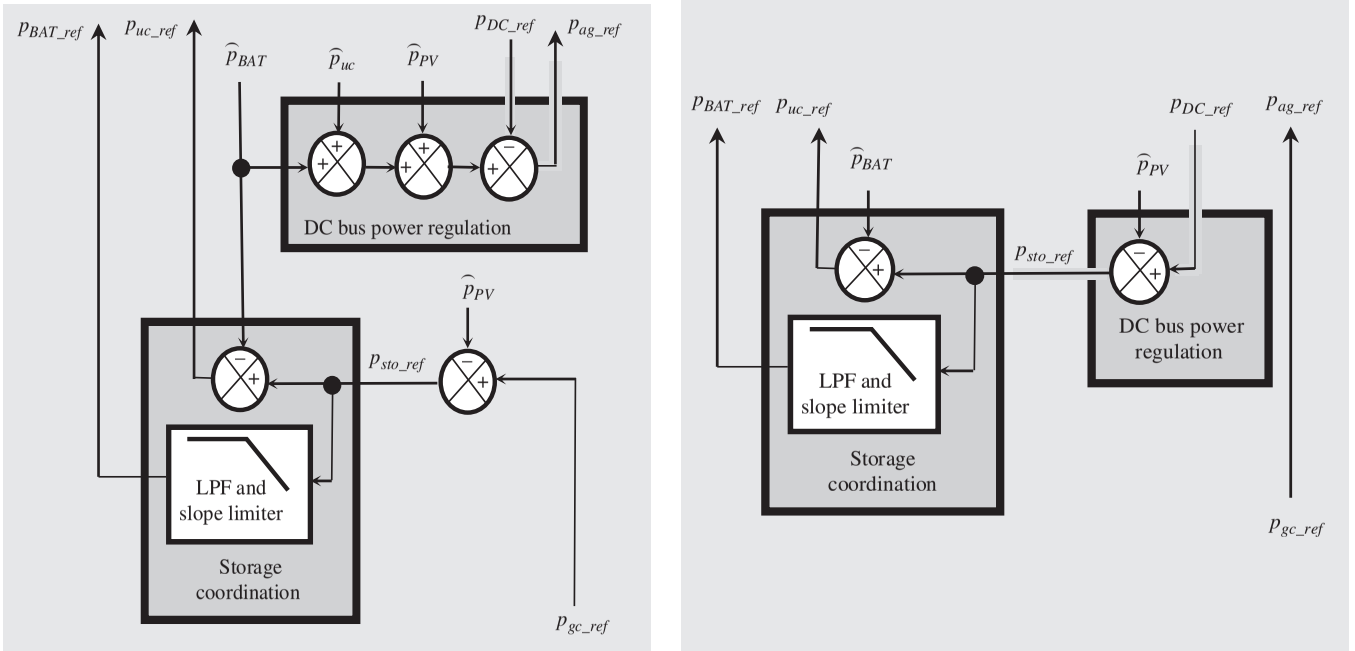

Figure 1.44 Operation strategies: (a) grid-following strategy and (b) source supplying strategy.

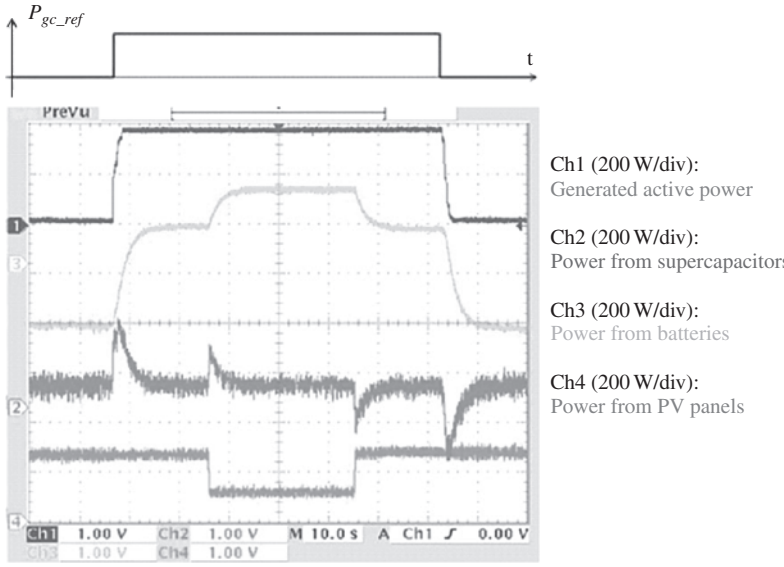

Figure 1.45 Experimental results for an active PV generator.

records are shown in Fig. 1.45. The PV power production changes between fourth and seventh second from 250 to 100 W. During the test, the batteries cannot immediately supply all the surplus production when the PV power production changes or when the PV production decreases fast, so the ultracapacitors help to perform the power balancing.

Next scenario is done at night, when there is no electrical production from PV power. Figure 1.46 shows the variation of the grid power and the dynamic currents from both storage units. When a step change from 0 to 200 W occurs in the grid load demand (p_g) at the 19 s, the batteries are discharged with a slow power increase and, at the same time, the ultracapacitors are instantaneously discharged with a high current to meet the grid load demand (Fig. 1.46).

1.4.4 Control of Grid-Connected Solar Power Inverters: A Review

Over the years, the PWM converters have drastically increased their importance on the market of energy conversion for PV applications. Two technology breakthroughs enabled these remarkable developments: (i) innovations in the field of power electronics, which brings improvements in efficiency (reduction of switching losses), power density, power quality, common mode voltage, electromagnetic interference, and so on; (ii) innovations in the field of control schemes, which currently contain many sophisticated control functions (Fig. 1.47), for example, inner current/power and outer DC-link controls, MPPT, monitoring and grid synchronization, special control functions for

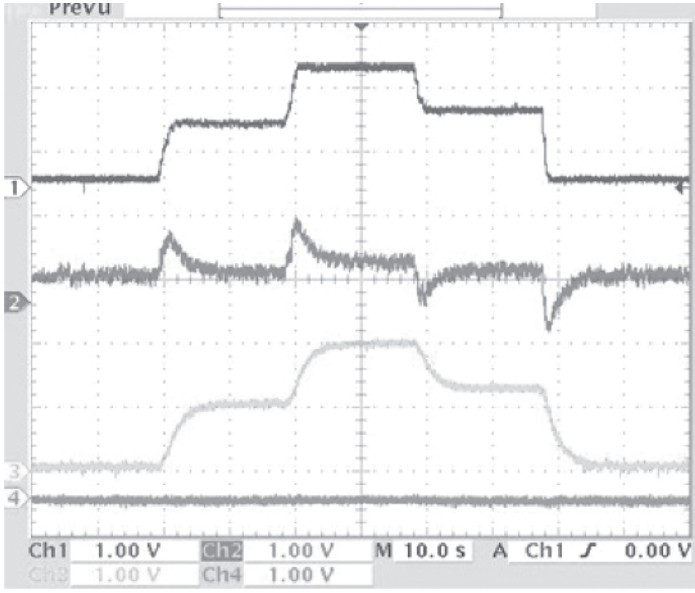

Ch1 (200 W/div): p_g; Ch2 (200 W/div): p_{uc}; Ch3 (200 W/div): p_{bat}; Ch4 (200 W/div): p_{PV}

Figure 1.46 Experimental results in the nighttime.

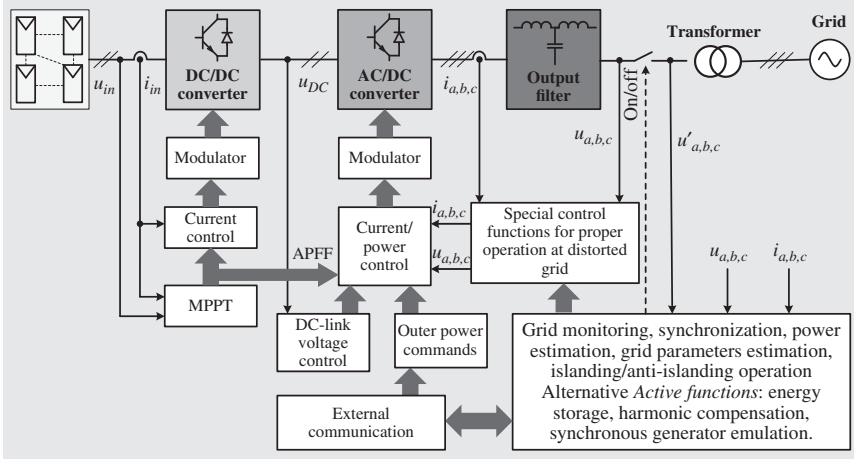

Figure 1.47 General control structure of a grid-connected SPG. *Source*: Cadaval *et al.*, 2015 [20]. Reproduced with permission of IEEE.

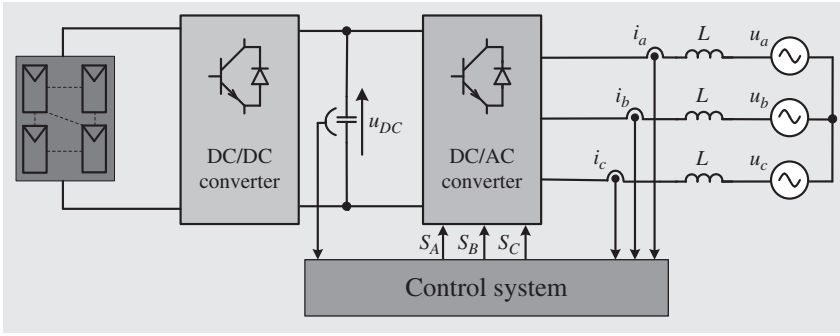

Figure 1.48 Simplified DC/AC PWM converter structure.

proper operation at significantly distorted grid, islanding/anti-islanding operation, active power feedforward, outer control loop for active/reactive power control to support power system, energy storage, harmonic compensation, and synchronous generator emulation [24–28].

Recently, various inner control algorithms have been proposed in recent works for the type of DC/AC PWM converters in MW PV applications [24, 29], but many of them are still under way and they have not yet placed in industry. Therefore, using the simplified system structure shown in Fig. 1.48, this section only describes the most promising and attractive methods for industry such as voltage-oriented control (VOC), direct power control space vector modulated (DPC-SVM), and predictive control (PC) approaches.

The conventional VOC uses the closed-loop current control in the rotating reference frame. A characteristic feature for this current controller is the processing of signals in two coordinate systems (Fig. 1.49), after converting

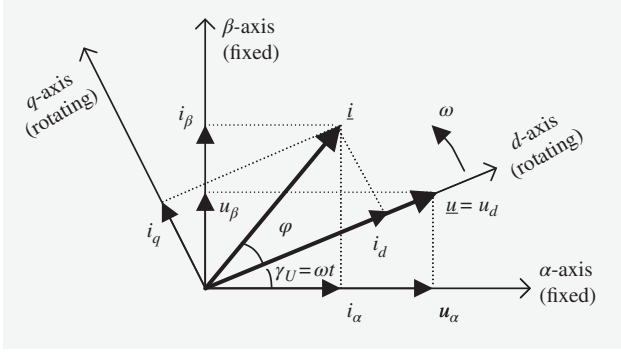

Figure 1.49 Coordinate transformation of line current and voltage from the stationary α–β to the rotating d–q coordinates.

three-phase measured values to the equivalent two-phase system α–β and then to the rotating d–q coordinate system via a α–β/d–q block [29].

As the d–q frame rotates with the same speed as the electrical quantities, the projected coordinates are DC signals. In the voltage-oriented d–q frame, the AC grid current vector $\underline{i}$ is split into two rectangular components $\underline{i} = [i_d, i_q]$. The component i_q determines indirectly the reactive power, whereas i_d decides indirectly the active power flow. Thus, the reactive and active powers can be controlled independently.

The unity power flow (UPF) condition is met when the grid current vector $\underline{i}$ is aligned with the grid voltage vector $\underline{u}$, which means that the q-axis current should be set to zero in all cases, while the reference current i_d is set by the DC-link voltage controller and controls the active power flow. As shown in Fig. 1.50a, the output signals from PI controllers after a $dq/\alpha\beta$ transformation are used to generate switching signals via a space vector modulator (SVM).

An important drawback of the VOC is the algorithm complexity (many coordinate transformations are needed) as well as the sensitivity to the grid voltage distortion. The last drawback can be eliminated, but it significantly complicates the algorithm [26]. The VOC can be also realized in the stationary α–β coordinate system, but PI controllers cannot be used for current regulation because they result in a steady-state error. However, this can be solved by replacing PI current regulators with proportional/resonant (PR) controllers, which consist of a proportional gain and a resonant integrator. The transfer function of a PR controller contains a pair of conjugate poles tuned at the fundamental grid frequency ω, which allows perfect tracking of sinusoidal signals without any error.

A basic block diagram of the VOC in the stationary coordinate system is shown in Fig. 1.50b and it is based on an inner current control loop with PR and an outer voltage control loop with PI. The commanded DC-link voltage u_{DC_ref} is compared with the measured u_{DC} voltage. The error is delivered to the PI controller, which generates the amplitude of the commanded current i_{DC_ref}. Next, this current is multiplied by the angle of the line voltage u_L as $\cos(\omega t)$ and $\sin(\omega t)$ to get i_{α_ref} and i_{β_ref}. These reference current signals in the stationary coordinate system are compared with the measured grid currents i_α and i_β and the errors are delivered to the PR controller. The outputs of the PR controller are directly (without transformation) used to generate switching signals by an SVM. An interesting feature of this control is the proper operation under distorted grid voltages by connecting multiple PR compensators, which are tuned at specific high-order harmonics, for example, fifth, seventh, in parallel [30].

Another less known method is direct power control-space vector modulated (DPC-SVM), which uses inner loops of active and reactive power control (Fig. 1.50c) [31]. The commanded reactive power q_{ref} (set to zero for UPF operation) and active power p_{ref} values (delivered from the outer PI-DC voltage controller) are compared with the estimated q and p values, respectively. The errors are delivered to PI controllers to eliminate steady-state errors because

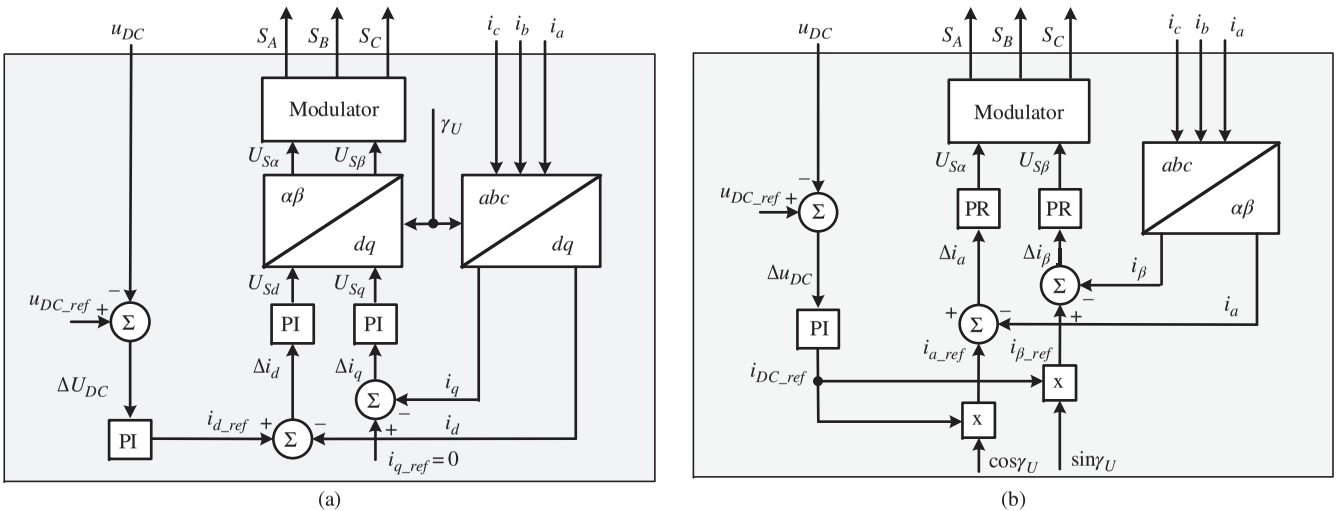

Figure 1.50 Control system schemes: (a) VOC in the synchronous rotating coordinate system, (b) VOC in the stationary coordinate system, (c) direct power control with the space vector modulator (DPC-SVM), and (d) model predictive control (MPC). *Source*: Cadaval *et al.*, 2015 [20]. Reproduced with permission of IEEE.

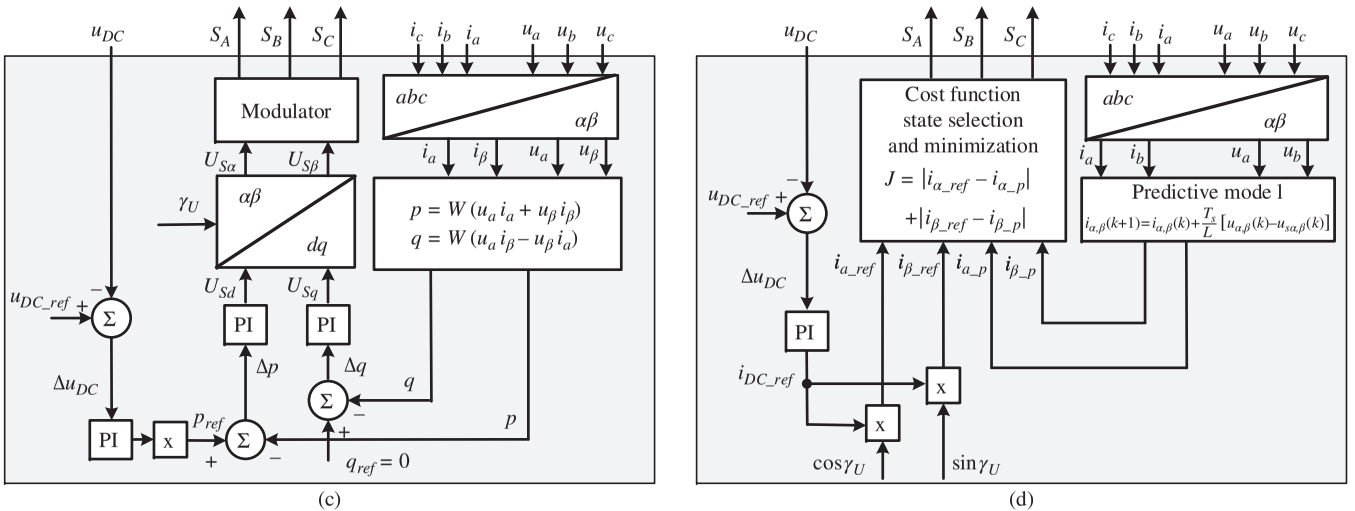

Figure 1.50 (*Continued*)

they are DC quantities. The output signals from the PI controllers after transformation from the stationary to synchronous rotating coordinates are used to generate switching signals by an SVM.

Recently, a control scheme called model predictive control (MPC) (Fig. 1.50d) has been applied to control inverters. It is based on the mathematical model of the controlled system and the calculation (prediction) of future values of the state variables. It is assumed that the system can represent a finite number of states in every time period [32]. Thus, first of all, the model must be as accurate as possible because the control performance is highly dependent on the parameters. Using measured values of grid currents, their values in the forthcoming sampling can be calculated, with respect to available control states. It must be done for all switching states in each iteration of the algorithm.

Some features of PC are very interesting, for example, fast dynamics and the capability of dealing with multiple constraints, which is attractive especially for high power converters operating at very low switching frequency (500–1000 Hz). Similar to other methods, the MPC has also some drawbacks, for example, variable switching frequency (causing difficulties for the design of the LC input EMI filter), high sampling frequency needed for digital implementation (demand of fast microprocessor), and sensitivity to parameter variations of the grid filter, which cause difficulties in implementing MPC in industry. The advantages and features of the control schemes described above are summarized in Table 1.3 [20].

Table 1.3 Advantages and features of control schemes for DC/AC converter in PV applications.

		VOC (Fig. 50a)	VOC (Fig. 1.50b)	DPC-SVM (Fig. 1.50c)	MPC (Fig.1.50d)
Operation in stationary coordinate system		No	Yes	Yes/no	Yes
Power control – indirect		Yes	Yes	No	Yes
Power control – direct		No	No	Yes	No
Constant switching frequency		Yes	Yes	Yes	No
Low algorithm complexity		No	Yes/no	Yes/no	Yes
Low computation intensity		Yes	Yes	Yes	No
Low sensitivity to line inductance variation		Yes	Yes	Yes	No
Low sensitivity to line voltage distortion	THD of line current	No	Yes	Yes	No
	Power factor	Yes	No	No	Yes

1.5 Summary

This chapter addressed the integration of RESs and described the fundamentals of PV and wind energy conversion systems. The relevant characteristics and control structures were discussed. The average models for the wind and PV-based active generators (WPG and SPG) were obtained. The modeling of these complex generation systems were led by considering each source with the dedicated power electronic converters. For the design of relevant control schemes in each energy conversion system, a hierarchical control structure was used.

The results were evaluated using simulations and laboratory experiments. The performed simulations showed the performances of the modeling and control structures. Experimental test results verified the effectiveness of the outcomes and showed desirable dynamic performances.

References

1 United Nations Environment Program (1997) Kyoto Protocol, http://www.kyotoprotocol.com.
2 International Energy Agency (IEA) (2015) Energy and Climate Change, World Energy Outlook Special Report, http://www.iea.org/publications/freepublications/publication/weo-2015-special-report-energy-climate-change.html.
3 Zhong, Q.-C. and Hornik, T. (2013) *Control of Power Inverters in Renewable Energy and Smart Grid Integration*, Wiley, Hoboken, NJ.
4 Bevrani, H., Watanabe, M., and Mitani, Y. (2014) *Power System Monitoring and Control*, IEEE-Wiley Press, New York.
5 Bevrani, H., Ghosh, A., and Ledwich, G. (2010) Renewable energy sources and frequency regulation: survey and new perspectives. *IET Renewable Power Generation*, **4** (5), 438–457.
6 Robyans, B., Francois, B., Delille, G., and Saudemont, C. (2015) *Energy Storage in Electric Power Grids*, Wiley.
7 Blaabjerg, F., Teodorescu, R., Liserre, M., and Timbus, A.V. (2006) Overview of control and grid synchronization for distributed power generation systems. *IEEE Transactions on Industrial Electronics*, **53** (5), 398–1409.
8 Ataee, S., Khezri, R., Feizi, M. R., and Bevrani, H. (2015) *Impacts of Wind and Conventional Power Coordination on the Short-Term Frequency Performance*. 23rd Iranian Conference on Electrical Engineering ICEE, Tehran, Iran.

9 Khezri, R. and Bevrani, H. (2015) Voltage performance enhancement of DFIG-based wind farms integrated in large-scale power systems: coordinated AVR and PSS. *International Journal of Electrical Power and Energy Systems*, **73**, 400–410.

10 Saleh, M. and Bevrani, H. (2011) Dynamic analysis and stability improvement concerning the integration of wind farms: Kurdistan electric network case study, in *Innovation in Power, Control and Optimization: Emerging Energy Technologies* (eds P. Vasant, N. Barsoum, and J. Webb), IGI Global, pp. 198–219. Chapter 6.

11 Bouscayrol, A. and Delarue, P. (2002) Simplifications of the maximum control structure of a wind energy conversion system with an induction generator. *International Journal of Renewable Energy Engineering*, **4** (2), 479–485.

12 Li, P. (2010) Design and control of a PV active generator with integrated energy storages: application to the aggregation of producers and consumers in an urban micro smart grid. PhD thesis, Ecole Centrale de Lille, France.

13 Onar, O.C., Uzunoglu, M., and Alam, M.S. (2006) Dynamic modeling design and simulation of a wind/fuel cell/ultra-capacitor-based hybrid power generation system. *International Journal of Power Sources*, **161** (1), 707–722.

14 Zhou, T. (2009) Control and energy management of a hybrid active wind generator including energy storage system with super-capacitors and hydrogen technologies for microgrid application. PhD thesis, Ecole Centrale de Lille, France.

15 Robyns, B., Davigny, A., François, B. *et al.* (2012) *Electricity Production from Renewables Energies*, Wiley.

16 Bevrani, H. (2014) *Robust Power System Frequency Control*, 2nd edn, Springer.

17 Li, P., Degobert, P., Robyns, B., and Francois, B. (2008) Implementation of interactivity across a resilient microgrid for power supply and exchange with an active distribution network. CIRED Seminar 2008: SmartGrids for Distribution, Frankfurt.

18 Fakham, H., Lu, D., and Francois, B. (2011) Power control design of a battery charger in a hybrid active PV generator for load-following applications. *IEEE Transactions on Industrial Electronics*, **58** (1), 95–104.

19 Lu, D. (2010) Design and control of a PV active generator with integrated energy storages: application to the aggregation of producers and consumers in an urban micro smart grid. PhD thesis, Ecole Centrale de Lille, France.

20 Cadaval, E.R., Francois, B., Malinowski, M., and Zhong, Q.C. (2015) Grid-connected photovoltaic plants: an alternative energy source, replacing conventional sources. *IEEE Industrial Electronics Magazine*, **9** (1), 18–32.

21 Kanchev, H., Lu, D., Colas, F. *et al.* (2011) Energy management and power planning of a microgrid with a PV-based active generator for smart grid applications. *IEEE Transactions on Industrial Electronics*, **58** (10), 4583–4592.

22 Lu, D., Fakham, H., Zhou, T., and Francois, B. (2010) Application of Petri nets for the energy management of a photovoltaic based power station including storage units. *Renewable Energy*, **35** (6), 1117–1124.

23 Xingyu, Y., Abbes, D., Bevrani, H., and Francois, B. (2016) *Day-Ahead Optimal and Reserve Power Dispatching in PV Based Urban Microgrid*. 18th European Conference on Power Electronics and Applications-EPE'16 ECCE, Karlsruhe, Germany, 5–9 September 2016.

24 Wilamowski, B. and Irwin, D. (2011) *Industrial Electronics Handbook*, Taylor & Francis Group.

25 Bevrani, H. (2012) Microgrid controls, in *Standard Handbook for Electrical Engineers*, 16th edn (ed. H. Wayne Beaty), McGraw-Hill, pp. 160–176 Section 16.9.

26 Kazmierkowski, M.P., Jasinski, M., and Wrona, G. (2011) DSP-based control of grid-connected power converters operating under grid distortions. *IEEE Transactions on Industrial Informatics*, **7** (2), 204–211.

27 Teodorescu, R., Liserre, M., and Rodríguez, P. (2011) *Grid Converters for Photovoltaic and Wind Power Systems*, Wiley-IEEE Press.

28 Guerrero, J.M., Chandorkar, M., Lee, T.-L., and Loh, P.C. (2013) Advanced control architectures for intelligent microgrids – Part I: decentralized and hierarchical control. *IEEE Transactions on Industrial Electronics*, **60** (3), 1254–1262.

29 Malinowski, M., Kazmierkowski, M.P., and Trzynadlowski, A. (2003) A comparative study of control techniques for PWM rectifiers in AC adjustable speed drives. *IEEE Transactions on Power Electronics*, **18** (6), 1390–1396.

30 Abu-Rub, H., Malinowski, M., and Al-Hadad, K. (2014) Power electronics for renewable energy systems, transportation and industrial applications, in *Photovoltaic Energy Conversion Systems* (eds S. Kouro, B. Wu, H. Abu-Rub, and F. Blaabjerg), Wiley, Hoboken, NJ, Chapter 7.

31 Malinowski, M., Jasinski, M., and Kazmierkowski, M.P. (2004) Simple direct power control of three-phase PWM rectifier using space-vector modulation (DPC-SVM). *IEEE Transactions on Industrial Electronics*, **51** (2), 447–454.

32 Rodriguez, J. and Cortes, P. (2012) *Predictive control of power converters and electrical drives*, Wiley, Hoboken, NJ.